NUSC Technical Report 6815
1 October 1982

Detection Performance Characteristics for a System With Quantizers, Or-ing, and Accumulator

Albert H. Nuttall
Surface Ship Sonar Department

OCT 2 7 1982
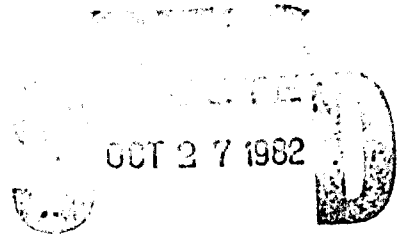
A

Naval Underwater Systems Center
Newport, Rhode Island / New London, Connecticut

Preface

This research was conducted under NUSC Project No. B12014, Subproject No. S0219-AS, *AN/BQQ-5 Passive Systems Engineering*, Principal Investigator Seymour M. Kessler (Code 3213), Program Manager CAPT Van Metre, NAVSEA (PMS 409). Also, this research was conducted under NUSC Project No. A75205, Subproject No. ZR0000101, *Applications of Statistical Communication Theory to Acoustic Signal Processing*, Principal Investigator Dr. Albert H. Nuttall (Code 3302), Program Manager Mr. Robert M. Hillyer, Naval Material Command (MAT 05).

The Technical Reviewer for this report was Seymour M. Kessler (Code 3213).

Reviewed and Approved: 1 October 1982

W. A. VonWinkle
Associate Technical Director
for Technology

The author of this report is located at the New London
Laboratory, Naval Underwater Systems Center,
New London, Connecticut, 06320

REPORT DOCUMENTATION PAGE		READ INSTRUCTIONS BEFORE COMPLETING FORM
1. REPORT NUMBER TR 6815	2. GOVT ACCESSION NO. AD-A120 794	3. RECIPIENT'S CATALOG NUMBER
4. TITLE (and Subtitle) DETECTION PERFORMANCE CHARACTERISTICS FOR A SYSTEM WITH QUANTIZERS, OR-ING, AND ACCUMULATOR		5. TYPE OF REPORT & PERIOD COVERED
		6. PERFORMING ORG. REPORT NUMBER
7. AUTHOR(s) Albert H. Nuttall		8. CONTRACT OR GRANT NUMBER(s)
9. PERFORMING ORGANIZATION NAME AND ADDRESS Naval Underwater Systems Center New London Laboratory New London, Connecticut 06320		10. PROGRAM ELEMENT, PROJECT, TASK AREA & WORK UNIT NUMBERS B12014 A75205 S0219-AS ZR0000101
11. CONTROLLING OFFICE NAME AND ADDRESS Naval Material Command (MAT 05) Washington, D.C. 20360		12. REPORT DATE 1 October 1982
		13. NUMBER OF PAGES 66
14. MONITORING AGENCY NAME & ADDRESS (if different from Controlling Office)		15. SECURITY CLASS. (of this report) UNCLASSIFIED
		15a. DECLASSIFICATION / DOWNGRADING SCHEDULE
16. DISTRIBUTION STATEMENT (of this Report) Approved for public release; distribution unlimited.		
17. DISTRIBUTION STATEMENT (of the abstract entered in Block 20, if different from Report)		
18. SUPPLEMENTARY NOTES		

19. KEY WORDS (Continue on reverse side if necessary and identify by block numbers)

Detection Probability	Greatest	Exact Analysis	Optimum Processor
False Alarm Probability	Or-ing	Optimum Multi-Bit Quantizer	
Operating Characteristics	Accumulator	Discrete Fourier Transform	
Quantization	Multi-Channel	Exceedance Probability	
		Characteristic Functions	

20. ABSTRACT (Continue on reverse side if necessary and identify by block numbers)

The false alarm and detection probabilities of an N-channel system subject to L+1 level quantization, or-ing, and accumulation of M time samples, are evaluated exactly, with no Gaussian assumptions, for arbitrary values of N, L, M, and for a quantizer with arbitrary breakpoint locations. The channel noises are independent but can have arbitrary statistics. The signal occupies one unknown (possibly changing) channel, if present. Two FFTs suffice to sweep out a complete detection probability vs. threshold curve.

(over)

DD, FORM 1473

20. (Cont'd)

The optimum placement of quantizer breakpoints, for a fixed total number
of levels, L+1, is a subtle one and is shown to depend on N, M, and the
desired level of performance; a simple rule-of-thumb is presented which
yields near-optimum capability over the useful range of the operating
characteristics. A brief comparison with the optimum processor is made.

TABLE OF CONTENTS

LIST OF ILLUSTRATIONS

LIST OF SYMBOLS

N	number of input channels
m	sample time
$x_n(m)$	m-th time sample of n-th channel input waveform
M	number of time samples accumulated
L	number of quantizer abscissa breakpoints; $L+1$ is the number of quantizer output levels
$q\{\ \}$	quantizer nonlinear characteristic
b_ℓ	ℓ-th quantizer breakpoint location
$y(m)$	input to accumulator
z	output of accumulator; decision variable
$w(m)$	output of or-ing device in figure 5
$P_x^{(0)}$	cumulative distribution function of input x for signal absent
$P_x^{(1)}$	cumulative distribution function of input x for signal present
H_0, H_1	hypotheses 0 and 1: signal absent and present, respectively
P_w	cumulative distribution function of random variable w
α_ℓ	area of impulse at ℓ in the probability density function of random variable y
β_n	area of impulse at n in the probability density function of random variable z
f_z, f_y	characteristic functions of z and y, respectively
N_f	size of discrete Fourier transform; $N_f \geq ML+1$
J	integer-valued threshold
w_0, w_1	characteristic points of probability density function of w; figure 8
m_0, m_1	means of input x under H_0, H_1, respectively
σ	standard deviation of x
Φ	Gaussian cumulative distribution function; (17)
d_i	input deflection statistic; (18)
y_ℓ	normalized quantizer breakpoint; (20)
v	normalized variable; (23)
P_D, P_F	detection, false alarm probabilities, respectively

DETECTION PERFORMANCE CHARACTERISTICS FOR A
SYSTEM WITH QUANTIZERS, OR-ING, AND ACCUMULATOR

INTRODUCTION

Practical realizations of desired systems often incorporate approximations to the ideal processor or devices, for the sake of reduced expense and equipment complexity. In particular, quantization is frequently employed, since it facilitates data handling and processing in terms of storage and execution time. In addition, the large number of alternatives for signal presence and location that must be considered often dictates that data reduction procedures, sucn as or-ing, be adopted. Both of these suboptimum approaches, quantization and or-ing, degrade system performance, and it is important to know tne extent of the degradation. Alternatively, it is desirable to know how much the received signal strength must be increased in order to maintain a specified level of performance.

The effects of or-ing by itself were analyzed in ref. 1, where the required input signal-to-noise ratio for specified false alarm and detection probabilities was evaluated as a function of tne number of input channels and the observation time. In ref. 2, the additional degradation caused by the inclusion of quantization was derived, where the number of levels and breakpoint locations of tne quantizer were completely arbitrary. Both of these analyses, however, were limited to second-order moments of the decision variable, and were therefore most appropriate to the situation of large observation time and moderate false alarm probabilities. That is, the Gaussian presumption played a prevalent role in the analysis. A cursory study of good quantizer breakpoint locations was also given in ref. 2.

Numerical evaluation of tne or-ing losses, based upon the derivations in refs. 1 and 2 , were given in refs. 3 and 4, and a more extensive investigation of quantizer characteristics was conducted in ref. 5, which corroborated the results given in ref. 2. But again, all results were based on a second-order moment approach.

Here we will derive exact results for the false alarm and detection probabilities of a system with quantization, or-ing, and accumulation-in-time, for arbitrary input signal and noise statistics. Surprisingly, it turns out that inclusion of the additional nonlinearity (quantization) actually simplifies tne analysis, and the judicious use of FFTs (fast Fourier transforms) makes tne numerical evaluation of the probabilities an efficient and accurate procedure.

SYSTEM DESCRIPTION AND ASSUMPTIONS

The system of interest is depicted in figure 1. There are N input channels, each of which is subject to noise statistically independent of the other channel noises. A signal is either present on one (and only one) unknown input channel or it is not present at all; we wish to make a decision on presence versus absence with good quality. The input signal (if present) need not be additive to the input noise; all that is required is knowledge of the probability density function of the input channel random variable $x_n(m)$ (at sample time m) for signal present. By setting the signal strength to zero, we obtain the probability density function for noise-only, of course.

It is presumed that the signal, if present, remains so for all M discrete time samples accumulated at the or-ing output. However, the signal could remain in one channel, or it could wander over any number of channels in a deterministic or random manner, from time sample to time sample.

The probability density functions of inputs $\{x_n(m)\}$ are arbitrary except that they must be identical for all the noise-only channels. Extension to non-identically distributed channel noises appears possible but has not been pursued. No Gaussian assumptions are made at any point of the system of figure 1, for the general analysis to follow. However, the numerical example that we eventually pursue is for Gaussian inputs, although this could easily be replaced by a different case of interest; in fact, some candidate examples are listed later in an appendix.

Each channel input $x_n(m)$ is subject to memoryless quantization, where the quantizer output $q\{x_n(m)\}$ has a total of L+1 levels, and the L quantizer abscissa breakpoints are arbitrary; see figure 2. A general analysis for this most-general quantizer is possible and will be outlined later. We confine our attention here to the less-general quantizer depicted in figure 3, where the ordinate (output) levels are limited to the equi-spaced values 0, 1, 2, ..., L, but the abscissa (input) breakpoints $\{b_\ell\}$ are arbitrary, except that $b_\ell \leq b_{\ell+1}$ for $1 \leq \ell \leq L-1$, without loss of generality.

3
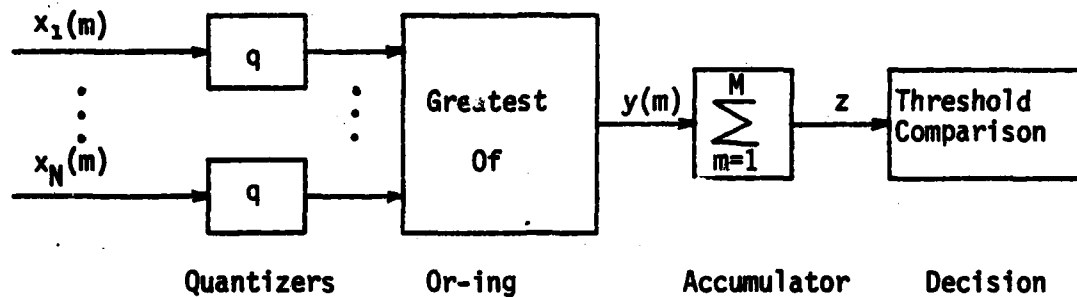
Figure 1.   Nonlinear System
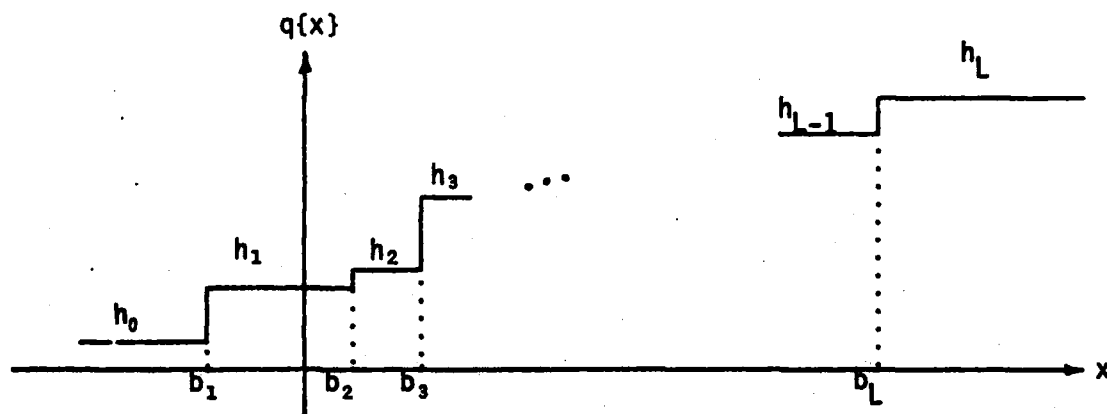
Figure 2.   General Quantizer Characteristic
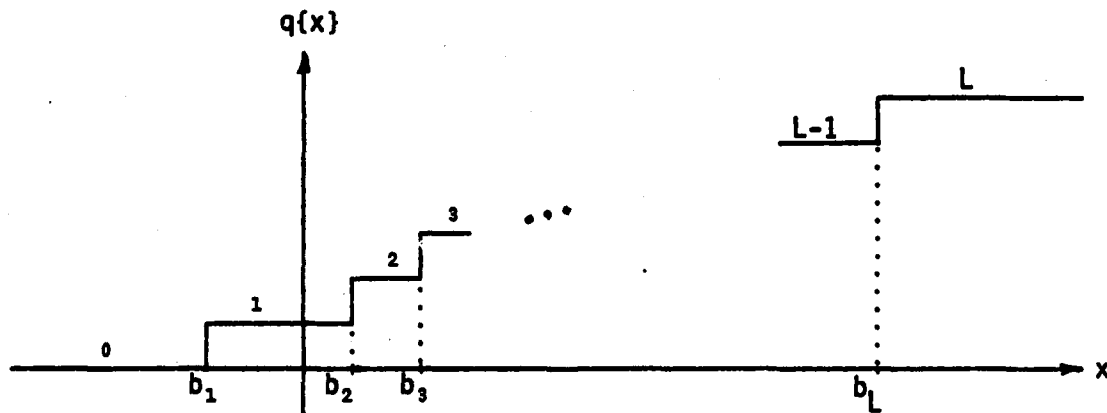
Figure 3.   Specific Quantizer Characteristic

This limitation on the possible quantizer output levels is not as restrictive as first appears. Reference to figure 1 quickly reveals that if the quantizer output levels were at equi-spaced values $h_0 + \ell \Delta h$, for $0 \le \ell \le L$, the operating characteristics, namely detection probability versus false alarm probability, would be completely <u>independent</u> of h_0 and $\Delta h \, (> 0)$. That is, h_0 and Δh affect the absolute scale of $y(m)$ and z, but they can be absorbed in a modified threshold at the system output. In fact, if one wants to approximate a given nonlinearity (such as $\tanh(x)$, for example) by a quantizer, L can be selected large enough, h_0 and Δh chosen without restriction, and the $\{b_\ell\}_0^L$ selected for a good fit. Then the analysis, as contained here for the quantizer of figure 3, applies directly, where h_0 and Δh (determined from the nonlinear fit) are discarded. h_0 and Δh are temporarily used for the fitting procedure, but are not fundamental to the system operating characteristics.

An example of a fit to $\tanh(x)$ is given in figure 4 for $L = 7$, where the
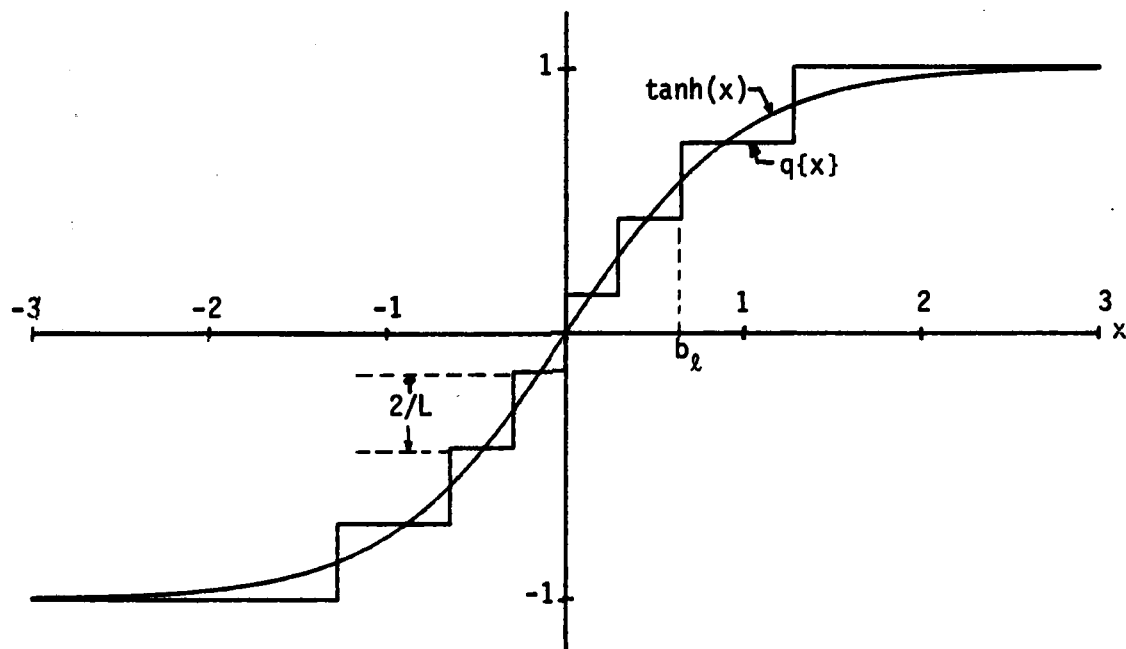
Figure 4. A Quantizer Fit to $\tanh(x)$ for $L = 7$

maximum ordinate error has been minimized and equalized at all the steps, and both functions approach ± 1 as x tends to $\pm \infty$. The best locations of the breakpoints are at

$$b_\ell = \frac{1}{2} \ln \left(\frac{\ell - \frac{1}{2}}{L + \frac{1}{2} - \ell} \right) \quad \text{for } 1 \leq \ell \leq L \quad , \tag{1}$$

for this example. We also have $h_0 = -1$, $\Delta h = 2/L$.

The or-ing device in figure 1 is subject to N inputs at each discrete time sample m. It selects the largest of these N random variables at each m and emits it to the accumulator as variable $y(m)$.

The accumulator adds up M input time samples to yield the decision variable

$$z = \sum_{m=1}^{M} y(m) \quad . \tag{2}$$

This output z is compared with a threshold. If the threshold is exceeded, a signal is declared present at the input to the system; otherwise, no signal is declared. For present analysis purposes, it is presumed that the discrete time samples (which can actually take place on the input channels) are sufficiently separated in time that the M random variables entering the accumulator are statistically independent.

When quantizer q in figure 1 is monotonically nondecreasing, the non-linear system in figure 1 is equivalent (for all inputs) to that shown in figure 5, where the quantization and or-ing operations have been interchanged.* The random variable $y(m)$ in figure 5 is identical to that in figure 1. We have added another random variable, $w(m)$, in figure 5 that has no counterpart in figure 1, for purposes of analysis. This interchange of operations is valid whether the quantizer of figures 2 or 3 is used.

Extensions of the above assumptions to more general situations, such as statistically dependent inputs or dependent accumulator samples, are discussed in ref. 2. However, the analysis there is limited to second-order moments, not threshold-crossing probabilities as considered here.

---

*See refs. 2 and 4 for two different proofs.
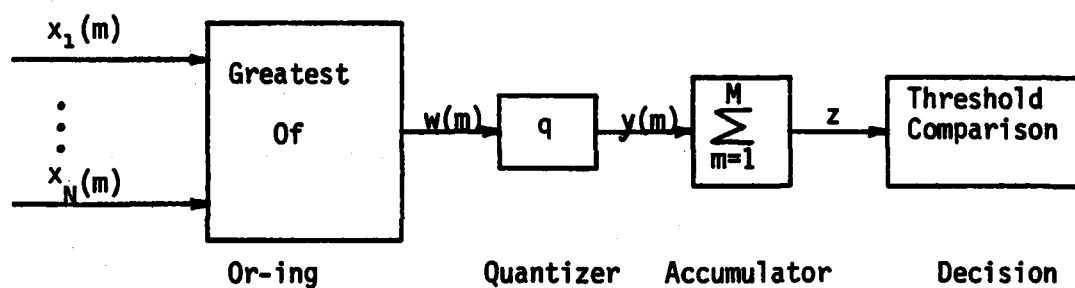
Figure 5.   Equivalent Nonlinear System
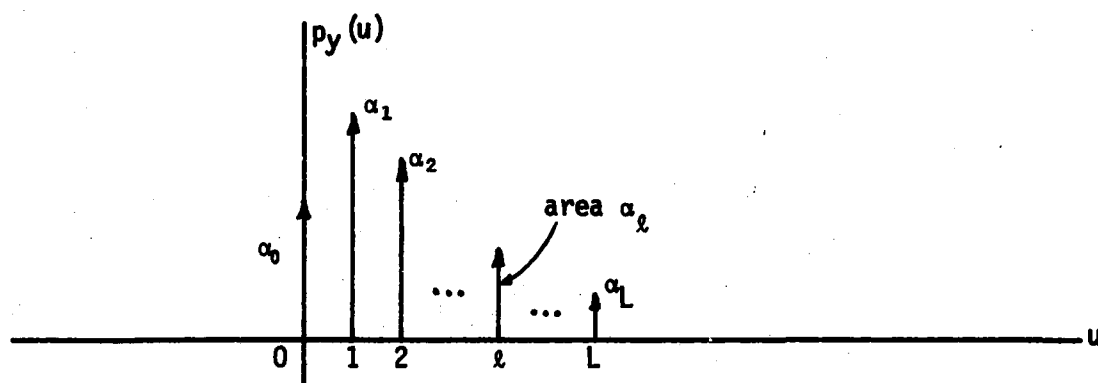
Figure 6.   Probability Density Function of y(m)
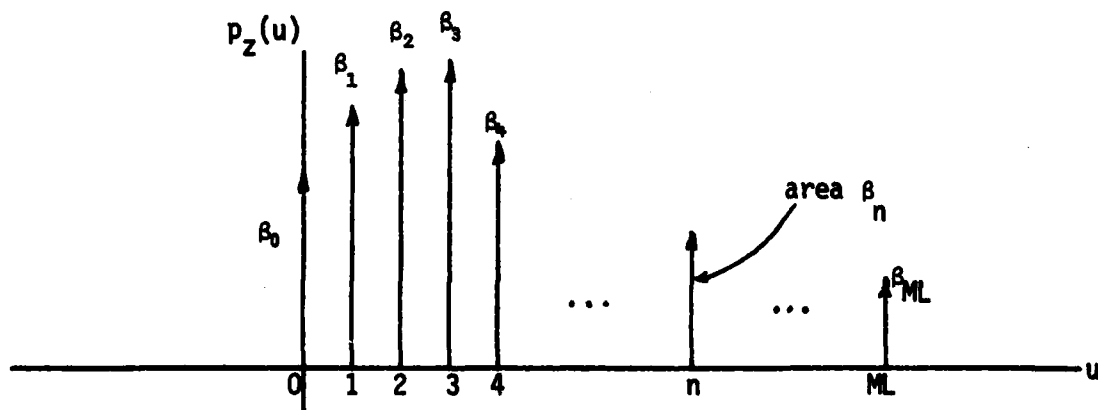
Figure 7.   Probability Density Function of z

ANALYSIS OF PERFORMANCE

In this section, we evaluate the false alarm and detection probabilities of the system in figure 5. The cumulative distribution function of an individual channel input, for signal absent, is $P_x^{(0)}$, where

$$P_x^{(0)}(u) = \text{Probability } (x < u | \text{signal absent}) \quad . \tag{3}$$

The cumulative distribution function of the channel input with signal-present is $P_x^{(1)}$. Both of these cumulative distribution functions are presumed known. The superscript will denote either hypothesis H_0 (no signal present) or hypothesis H_1 (signal present on that channel). Notice there is no restriction on the forms of $P_x^{(0)}$ or $P_x^{(1)}$; thus arbitrary input statistics (including nonadditive signals) are allowed. However, the noise-only channels are identically distributed.

Since the or-ing output in figure 5 is

$$w(m) = \max\{x_1(m), \ldots, x_N(m)\} \quad \text{for } 1 \le m \le M \quad , \tag{4}$$

tne cumulative distribution function of w(m) is, for any time instant m,

$$P_w(u) = \begin{cases} \left[P_x^{(0)}(u)\right]^N & \text{for } H_0 \\ \left[P_x^{(0)}(u)\right]^{N-1} P_x^{(1)}(u) & \text{for } H_1 \end{cases} , \tag{5}$$

since the signal (if present) is in only one (arbitrary) input channel. In fact, tne occupied cnannel can change from sample m to m+1, in a random or deterministic fashion, and (5) is still applicable.

The output y(m) of the quantizer in figure 5 is limited to the L+1 values $\ell = 0, 1, 2, \ldots, L$; see figure 3. Therefore the probability density function of random variable y(m) is impulsive, as shown in figure 6, where the area α_ℓ of the impulse at ℓ is given by

9

$$\alpha_\ell = \begin{cases} P_w(b_1) & \text{for } \ell = 0 \\ P_w(b_{\ell+1}) - P_w(b_\ell) & \text{for } 1 \leq \ell \leq L-1 \\ 1 - P_w(b_L) & \text{for } \ell = L \end{cases} \quad . \tag{6}$$

Here $\{b_\ell\}_1^L$ are the L abscissa breakpoints of the quantizer, and P_w is the cumulative distribution function of w, given by (5).

The output of the accumulator in figure 5 is called the decision variable and is given by the sum of M statistically independent random variables according to

$$z = \sum_{m=1}^{M} y(m) \quad . \tag{7}$$

Since $y(m)$ can only take on the values 0, 1, 2, ..., L, the decision variable z can only take on the values 0, 1, 2, ..., ML. Thus the probability density function of z is also impulsive, as depicted in figure 7; the area of the impulse at n is denoted by β_n.

We now need to relate the $\{\beta_n\}$ of figure 7 to the $\{\alpha_\ell\}$ of figure 6. To accomplish this, we resort to the characteristic functions of $y(m)$ and z. Using the statistical independence of the $\{y(m)\}$, the characteristic function of z is

$$f_z(\xi) = \overline{\exp(i\xi z)} = \left[\overline{\exp(i\xi y)}\right]^M = \left[f_y(\xi)\right]^M \quad , \tag{8}$$

where f_y is the characteristic function of random variable $y(m)$. But by use of figures 6 and 7, we have

$$f_y(\xi) = \int_{-\infty}^{\infty} du \; p_y(u) \exp(i\xi u) = \sum_{\ell=0}^{L} \alpha_\ell \exp(i\xi \ell) \quad , \tag{9}$$

and

$$f_z(\xi) = \int_{-\infty}^{\infty} du \; p_z(u) \exp(i\xi u) = \sum_{n=0}^{ML} \beta_n \exp(i\xi n) \quad . \tag{10}$$

Substitution of (9) and (10) in (8) yields

$$f_z(\xi) = \sum_{n=0}^{ML} \beta_n \exp(i\xi n) = \left[\sum_{\ell=0}^{L} \alpha_\ell \exp(i\xi \ell) \right]^M \quad . \tag{11}$$

Now the results of appendix A indicate that the set of numbers $\{\beta_n\}_0^{ML}$ can be recovered directly by an N_f-point DFT (discrete Fourier transform) of the set of characteristic function samples

$$f_z(2\pi n/N_f) \quad \text{for } 0 \le n \le N_f-1 \quad , \tag{12}$$

provided that

$$N_f \ge ML+1 \quad . \tag{13}$$

And from (11), we have the required characteristic function samples as

$$f_z(2\pi n/N_f) = \left[\sum_{\ell=0}^{L} \alpha_\ell \exp(i 2\pi n\ell/N_f) \right]^M \quad . \tag{14}$$

The sum on ℓ here is the conjugate of an N_f-point DFT of the L+1 real nonzero numbers $\{\alpha_\ell\}_0^L$ augmented by zeros. When this DFT is raised to the M-th power, it constitutes the required N_f samples of the characteristic function f_z that are needed for the DFT that leads to $\{\beta_n\}$.

To summarize, (5) yields the cumulative distribution function of w, and (6) gives the impulse areas $\{\alpha_\ell\}_0^L$. An N_f-point DFT of this sequence (augmented with zeros) is taken, then conjugated and raised to the M-th power. Another N_f-point DFT is then taken and the results divided by N_f. The end result is impulse areas $\{\beta_n\}$. The values returned (by the second DFT) for $\beta_{ML+1}, \ldots, \beta_{N_f-1}$ should all be zero, as should all the imaginary parts.

Although any value for N_f that satisfies (13) is permissible, the smallest power of 2 is most reasonable since then we can employ two FFTs above; this time-saving feature is employed here.

The probability that decision variable z equals or exceeds integer value J is, from figure 7,

$$\text{Probability} \left\{ z \geq J \right\} = \sum_{n=J}^{ML} \beta_n \qquad \text{for } 0 \leq J \leq ML \quad . \tag{15}$$

Tne above analysis for the exceedance probability in (15) is exact. When signal is present, (15) is the detection probability, whereas when signal is absent, (15) is the false alarm probability. The fundamental input statistics, $p_x^{(0)}$ and $p_x^{(1)}$, required in (5), are arbitrary.

QUANTIZER BREAKPOINT LOCATIONS

For a given number, $L+1$, of quantizer output levels, the selection of the L breakpoints $\{b_\ell\}$ should be done so as to optimize the performance of the system, that is, maximum detection probability for a specified false alarm probability. The equivalence of the two processors in figures 1 and 5 is the guide to good selection of the breakpoints; namely $\{b_\ell\}$ should lead to a maximum difference in outputs $y(m)$ for hypothesis H_1 vs. H_0. However, as figure 5 shows, this selection of $\{b_\ell\}$ is governed by the probability density functions of quantizer input w, not x; that is, the quantizer should take account of the or-ing nonlinearity and the number of input channels, N.

A problem arises here, however, in that the probability density functions of w under H_1 and H_0 depend on the particular value of input signal-to-noise ratio that obtains. Thus, the quantizer design should take the input signal-to-noise ratio into account. This situation is frequently encountered in likelihood ratio processing, in which the optimum processor often requires knowledge of absolute levels of input signal and noise. Since this knowledge is almost always lacking, a design that is good for representative values of input signal-to-noise ratio, that is, which correspond to adequate levels of performance, should be adopted. If the input signal-to-noise ratio is larger than these representative values, improved performance will result; if smaller, inadequate performance is expected anyway, regardless of quantizer breakpoint placements.

To get at the quantizer design, consider the probability density functions in figure 8 for random variable w under H_1 and H_0. w_0 is a point beyond which there is a small chance of w ever reaching under H_0; w_1 is a point below which w hardly ever reaches under H_1. Generally $w_1 < w_0$ for cases of practical importance; otherwise near-perfect performance is possible at this signal-to-noise ratio. Under H_0, we would like to locate the first breakpoint b_1 greater than w_0; then the false alarm probability would be substantially zero, regardless of the remaining $\{b_\ell\}$. On the other hand, under H_1, we would like to locate the last breakpoint b_L less than w_1; then the detection probability would be essentially 1.
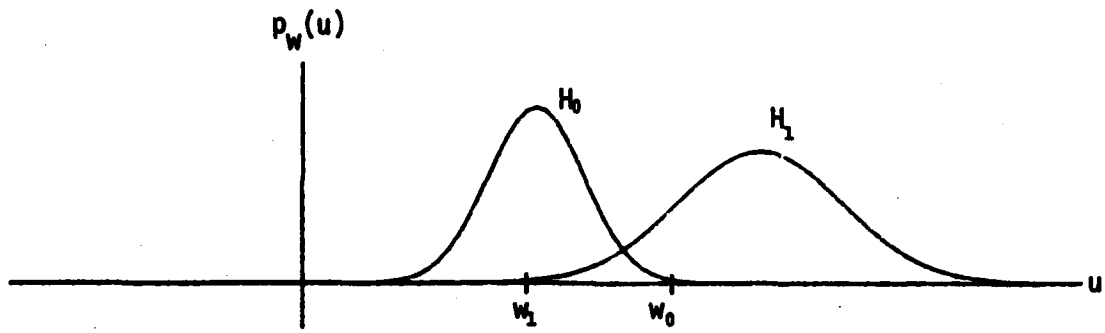
Figure 8. Probability Density Functions of w in figure 5
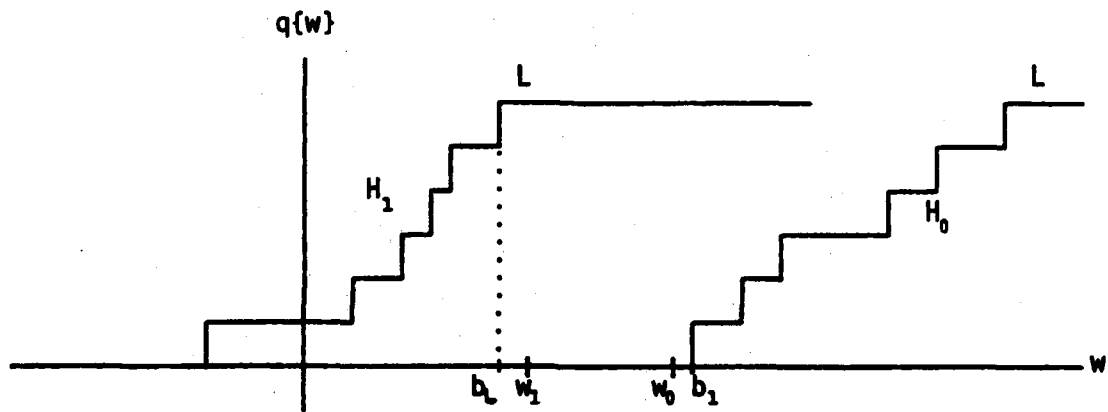


Figure 9. Desirable Quantizer Characteristics
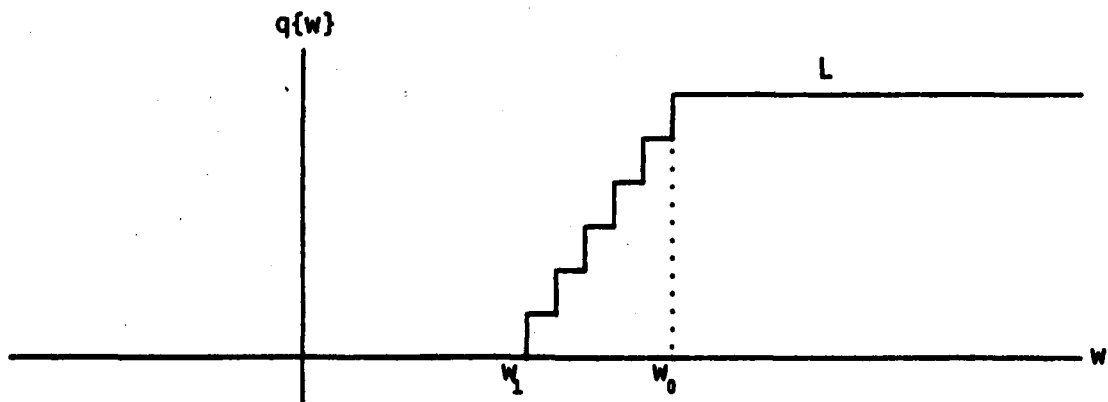
Figure 10. Compromise Quantizer Characteristic

These desirable quantizer characteristics under H_0 and H_1 are depicted
in figure 9. It is immediately seen that the desired features of both cases
can be realized for $w < w_1$ and $w > w_0$; that is, choose $q=0$ for $w < w_1$,
and choose $q=L$ for $w > w_0$. However there is an inherent conflict in the
intermediate region $w_1 < w < w_0$. The only way to strike a reasonable
compromise is to make q small near w_1 and make q large near w_0. That is,
locate the breakpoints in w_1, w_0, as indicated in figure 10. We shall
make them equally spaced on the input w, that is, $b_{\ell+1} - b_\ell$ independent of ℓ;
nonuniform abscissa spacings, such as in figure 4, are possible and could give
slightly better performance. However, sample computer runs have demonstrated
that for $L > 4$, essentially optimum performance is attained via uniform
breakpoint spacing. Also, for the larger values of input signal-to-
noise ratio, it will be shown that the optimum processor of the available
inputs takes precisely the form of figure 5, where the quantizer is replaced
by a linear gain.

The best quantizer placements in figure 10 obviously depend on the number,
N, of input channels and the input signal-to-noise ratio, since the
probability density functions of w displayed in figure 8 depend on these
quantities. But there is an additional less-obvious dependence on M, the
number of samples accumulated at the quantizer output. For larger M, the
separation of the probability density functions of z under H_0 and H_1 will
become better, if the input signal-to-noise ratio is held fixed. But often,
the larger values of M are employed so that lower input signal-to-noise ratios
can be tolerated and yet realize adequate performance levels; thus, the
probability density functions of w in figure 8 generally overlap more for the
larger values of M. This means that w_1 will be smaller and therefore the
breakpoints should be relocated. Further discussion of quantizer breakpoints
is deferred until the numerical investigation is undertaken.

INPUT STATISTICS

Up to now, the statistics of inputs $\{x_n\}$ in figures 1 and 5 have been arbitrary. We now specialize to the case of Gaussian noises; some other candidate statistics are given in appendix B. In particular, the cumulative distribution functions under H_0 and H_1 are

$$P_X^{(0)}(u) = \Phi\left(\frac{u-m_0}{\sigma}\right), \quad P_X^{(1)}(u) = \Phi\left(\frac{u-m_1}{\sigma}\right) , \tag{16}$$

respectively, where Φ is the Gaussian cumulative distribution function

$$\Phi(x) = \int_{-\infty}^{x} dt \ (2\pi)^{-1/2} \exp(-t^2/2) \equiv \int_{-\infty}^{x} dt \ \phi(t) . \tag{17}$$

The means of x_n are m_0 and m_1 under H_0 and H_1, respectively, while the standard deviation is the common value σ in both cases. For later use, we define the deflection statistic of the inputs as

$$d_i = \frac{m_1 - m_0}{\sigma} . \tag{18}$$

Reference to (5) and (6) indicates that we need the quantities

$$\left.\begin{aligned}
P_X^{(0)}\left(b_\ell\right) &= \Phi\left(\frac{b_\ell - m_0}{\sigma}\right) = \Phi\left(v_\ell\right) \\
P_X^{(1)}\left(b_\ell\right) &= \Phi\left(\frac{b_\ell - m_1}{\sigma}\right) = \Phi\left(v - d_i\right)
\end{aligned}\right\} \text{ for } 1 \leq \ell \leq L, \tag{19}$$

where we have used (16), (17), and defined the normalized breakpoints of the quantizer as

$$v_\ell = \frac{b_\ell - m_0}{\sigma} \quad \text{for } 1 \leq \ell \leq L . \tag{20}$$

Then (5) and (19) yield

$$P_w(b_\ell) = \begin{cases} \Phi^N(v_\ell) & \text{for } H_0 \\ \Phi^{N-1}(v_\ell)\Phi(v_\ell - d_i) & \text{for } H_1 \end{cases} \quad \text{for } 1 \leq \ell \leq L \quad . \qquad (21)$$

These are the quantities needed in (6) for the areas $\{a_\ell\}$ in figure 6. (If the noise standard deviations were σ_0 and σ_1 under H_0 and H_1, instead of the common σ in (16), the only changes would be to replace $v_\ell - d_i$ in the second line of (19) and (21) by $\frac{\sigma_0}{\sigma_1}\left(v_\ell - d_i\right)$). The results in the next section are based upon this Gaussian noise example.

RESULTS

By combining the general result for the cumulative distribution function of w in (5) with the Gaussian example in (16), we obtain

$$P_w(u) = \Phi^{N-1}\left(\frac{u-m_0}{\sigma}\right)\overline{\Phi}\left(\frac{u-m_1}{\sigma}\right)$$

$$= \Phi^{N-1}(v)\,\overline{\Phi}(v-d_1) \quad , \tag{22}$$

where we define normalized variable

$$v = \frac{u-m_0}{\sigma} \tag{23}$$

and have used (18). The probability density function of w under H_1 is

$$p_w(u) = \frac{d}{du}P_w(u) = \frac{1}{\sigma}\frac{d}{dv}\left\{\Phi^{N-1}(v)\,\overline{\Phi}(v-d_1)\right\}$$

$$= \frac{1}{\sigma}\left[(N-1)\,\overline{\Phi}(v-d_1)\,\phi(v) + \Phi(v)\phi(v-d_1)\right]\Phi^{N-2}(v) \quad , \tag{24}$$

where we used (17). This probability density function is plotted in figure 11
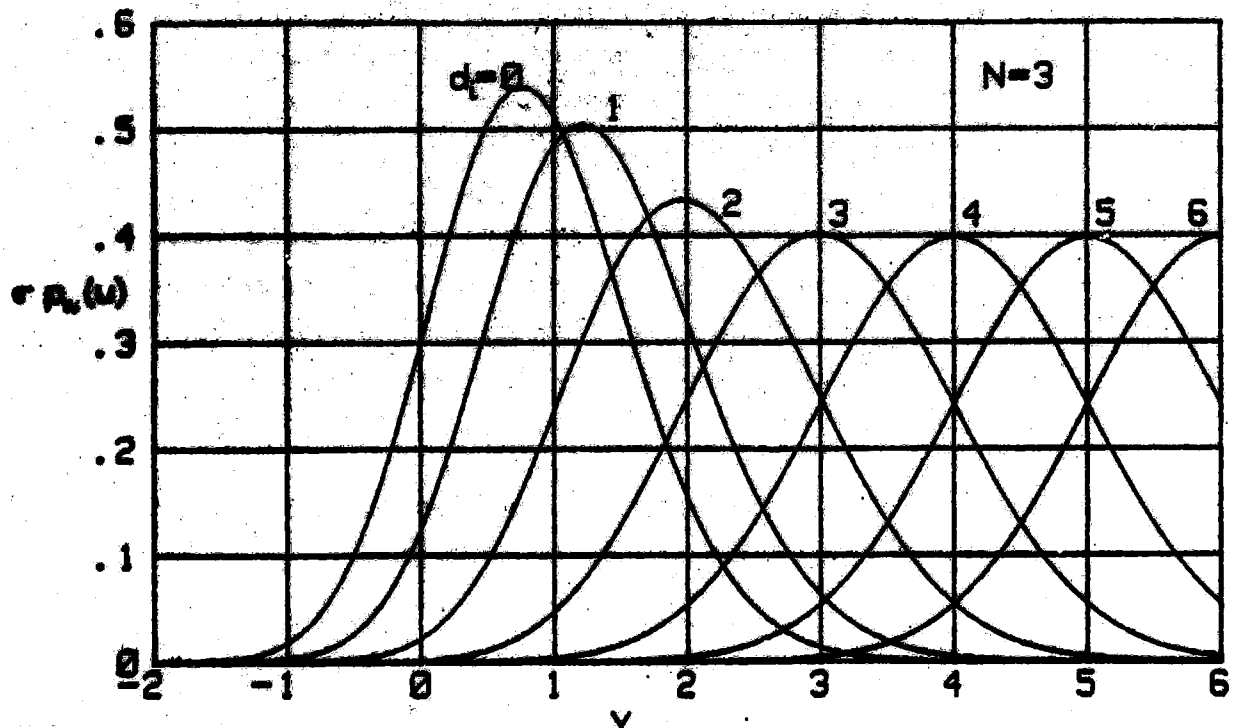
Figure 11. Probability Density Function of w for N = 3

for $N=3$ and several values of d_i. If we select, for example, $d_i=5$, the points w_1 and w_0 in figure 8 correspond approximately to $v = 1.4$ and 4.1 in figure 11. The curve for $d_i=0$ is the probability density function of w under H_0.

The false alarm probability, as given by (15) et seq., is plotted in figure 12 for an example with

$$N=3 \text{ input channels,}$$
$$M=5 \text{ time samples accumulated,}$$
$$L=7 \text{ quantizer breakpoints,}$$
$$\{v_\ell\} = 1.4(.45)4.1, \text{ normalized breakpoints.*} \tag{25}$$

(Since $L+1=8$ here, this is called a 3-bit quantizer.) Since threshold J can only take on integer values, the false alarm probability is only defined at those values, and is so indicated by crosses in figure 12. The detection probability P_D is plotted vs. the false alarm probability P_F, in figure 13,

by eliminating the parametric dependence of both on J. Again, both P_D and P_F are only defined at discrete points, as indicated by crosses; straight lines have been drawn between these points for ease of association of values. (In the curves to follow, these crosses are suppressed.) The program for the generation of figures 12 and 13 is given in appendix C.

The choice of breakpoints in (25) has realized near-optimum performance for $L=7$ and $d_i \approx 5$, in the upper-left corner of the plot. The curves for the smaller values of input signal-to-noise ratio, that is small d_i, are more crowded together; this reflects the usual small-signal suppression that is characteristic of nonlinear processors.

To demonstrate the effects of a bad choice of quantizer breakpoints, the previous example in (25) is rerun, with normalized breakpoints

$$\{v_\ell\} = 1,1,1,1,1,1,2, \tag{26}$$

instead of the uniform spacing. The results in figure 14 illustrate much poorer performance than figure 13, in addition to a very erratic appearance.

---

* The notation a(b)c denotes the sequence a, a+b, a+2b, ..., c-b, c.
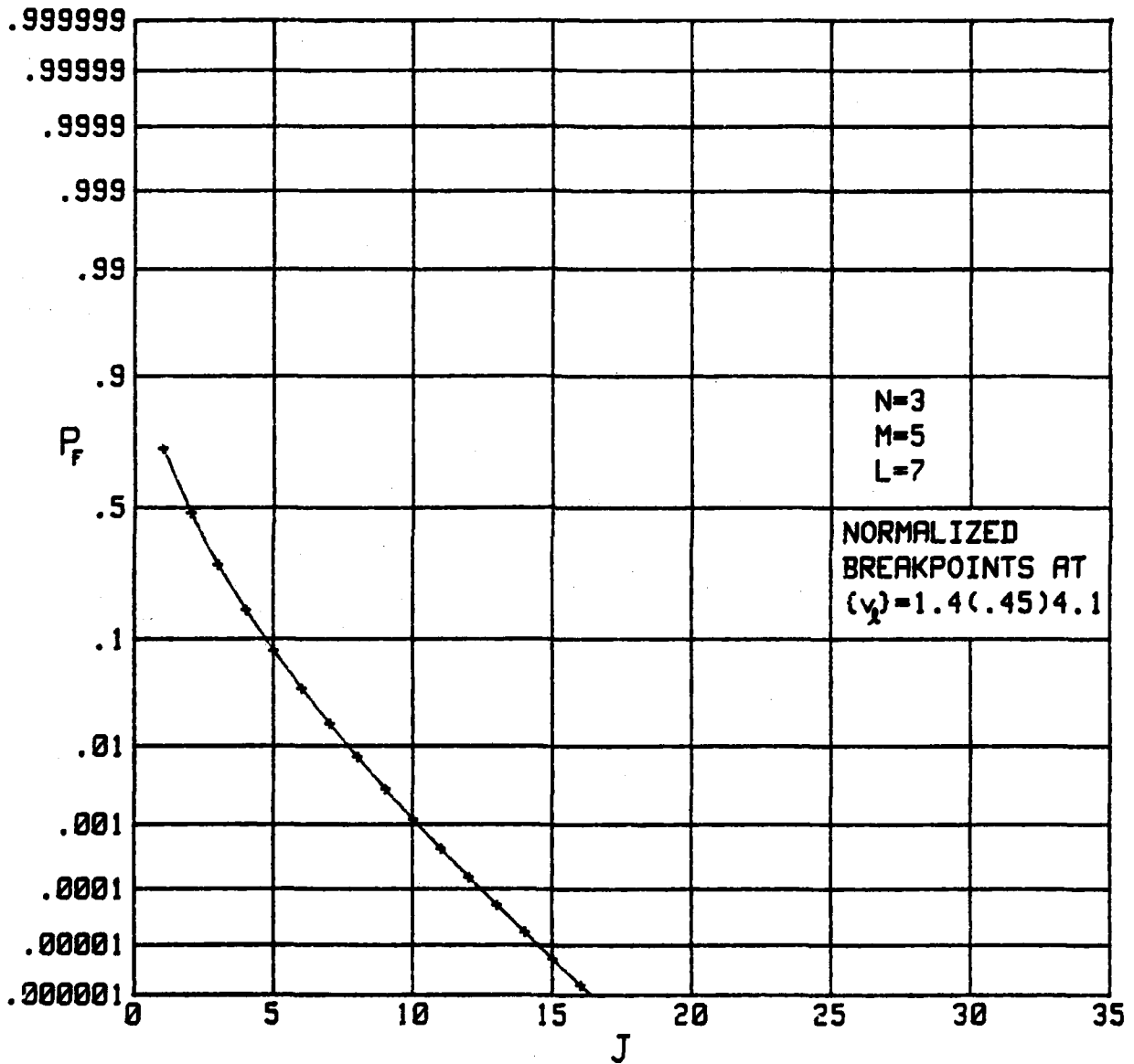
Figure 12. Probability of False Alarm vs. Threshold J
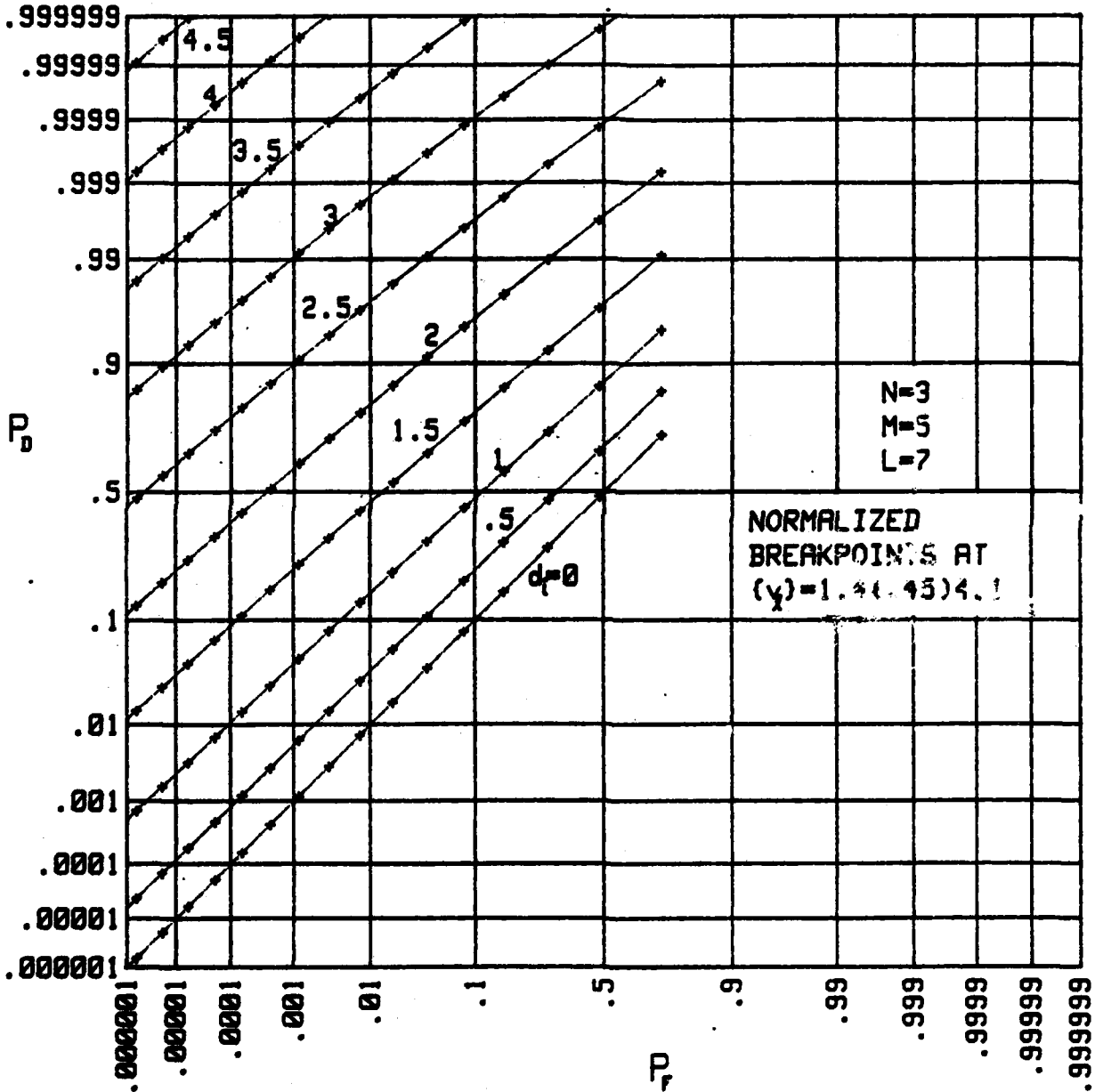
Figure 13.   Operating Characteristics for $\{v_\ell\}$ = 1.4(.45)4.1
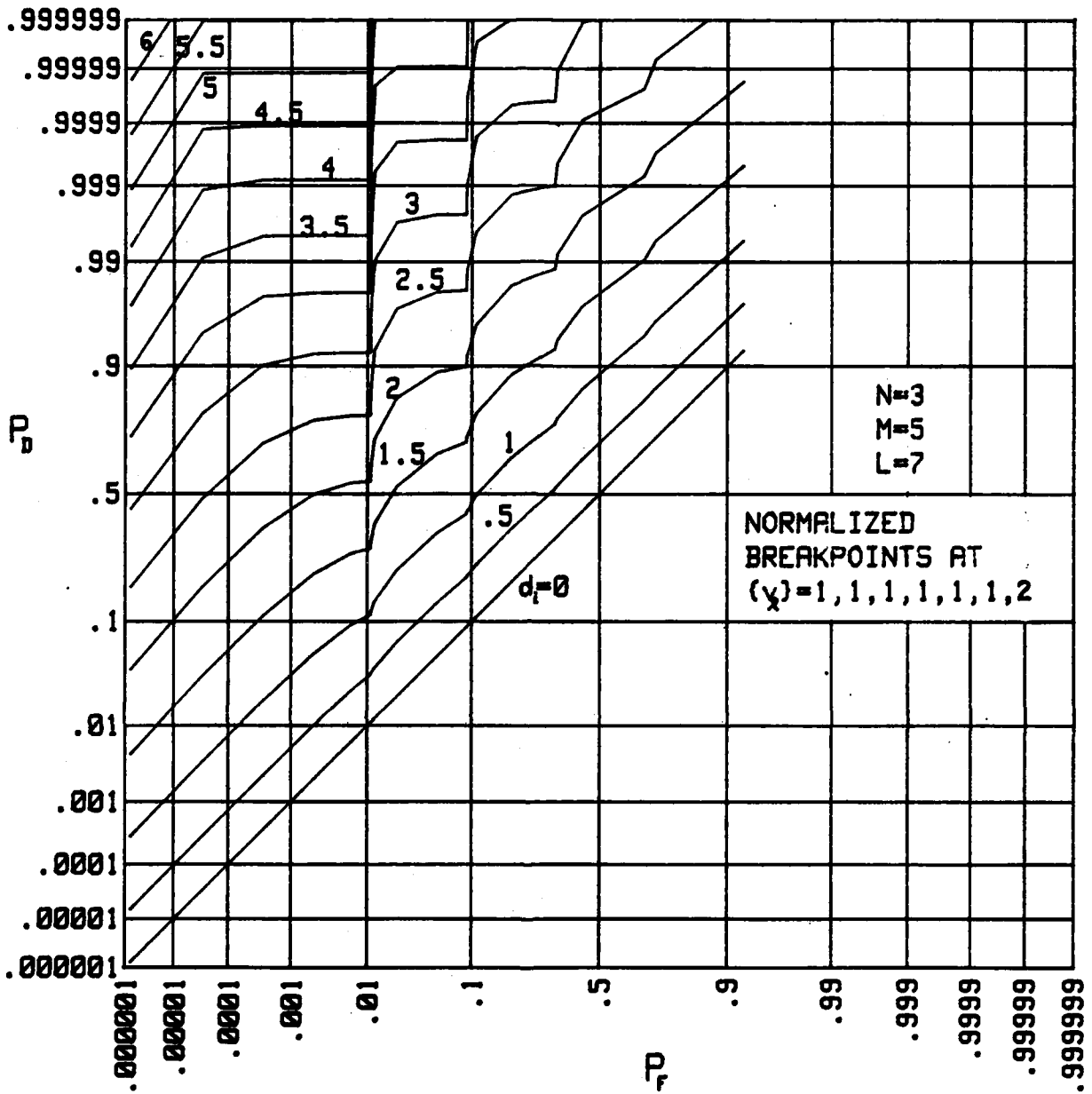
Figure 14. Operating Characteristics for $\{v_\lambda\}$ = 1,1,1,1,1,1,2

The curves for constant d_i must have a nonnegative slope, and never cross, but can have a wide variety of shapes. A similar bad placement for a 2-bit (L=3) quantizer is given in figure 15. This jagged behavior of the operating characteristic is typical when the breakpoints are bunched together instead of being uniformly spaced.

The next example is for

$$N=3, \quad M=16, \quad L=7, \quad \{v_\ell\} = 0(1/3) \, 2 \quad , \tag{27}$$

and is displayed in figure 16. This can be compared directly with the results of ref. 2, figure 5. Both require $d_i = 1.22$ for $P_F = 10^{-3}, P_D = .5$, and both require about $d_i = 1.75$ for $P_F = 10^{-6}$, $P_D = .5$. Thus the simplified analysis in ref. 2 is very reliable for large M, where it is reasonable to expect Gaussian statistics to hold.

In order to see if better performance is attainable by modifying the breakpoints, we return to the probability density function in figure 11 (for N=3) and observe that if we want to optimize for $d_i = 3$ (i.e., top left corner of figure 16), we should choose $w_1 \approx 0$, $w_2 \approx 4$. However, the narrowing effect on the decision-variable probability density function, due to the averaging caused by large M, indicated (by trial and error) that the best normalized breakpoints were

$$\{v_\ell\} = .5(.5)3.5 \quad . \tag{28}$$

The corresponding operating characteristic is displayed in figure 17; it is slightly better than figure 16. Thus the significant modification in normalized breakpoints from figure 16 to figure 17 did not yield significantly better performance, for this example with L=7.

The next example is run for comparison with ref. 2, figure 8. Namely we have

$$N=3, \quad M=32, \quad L=7 \quad , \tag{29}$$

and three different quantizer breakpoint sets:

24
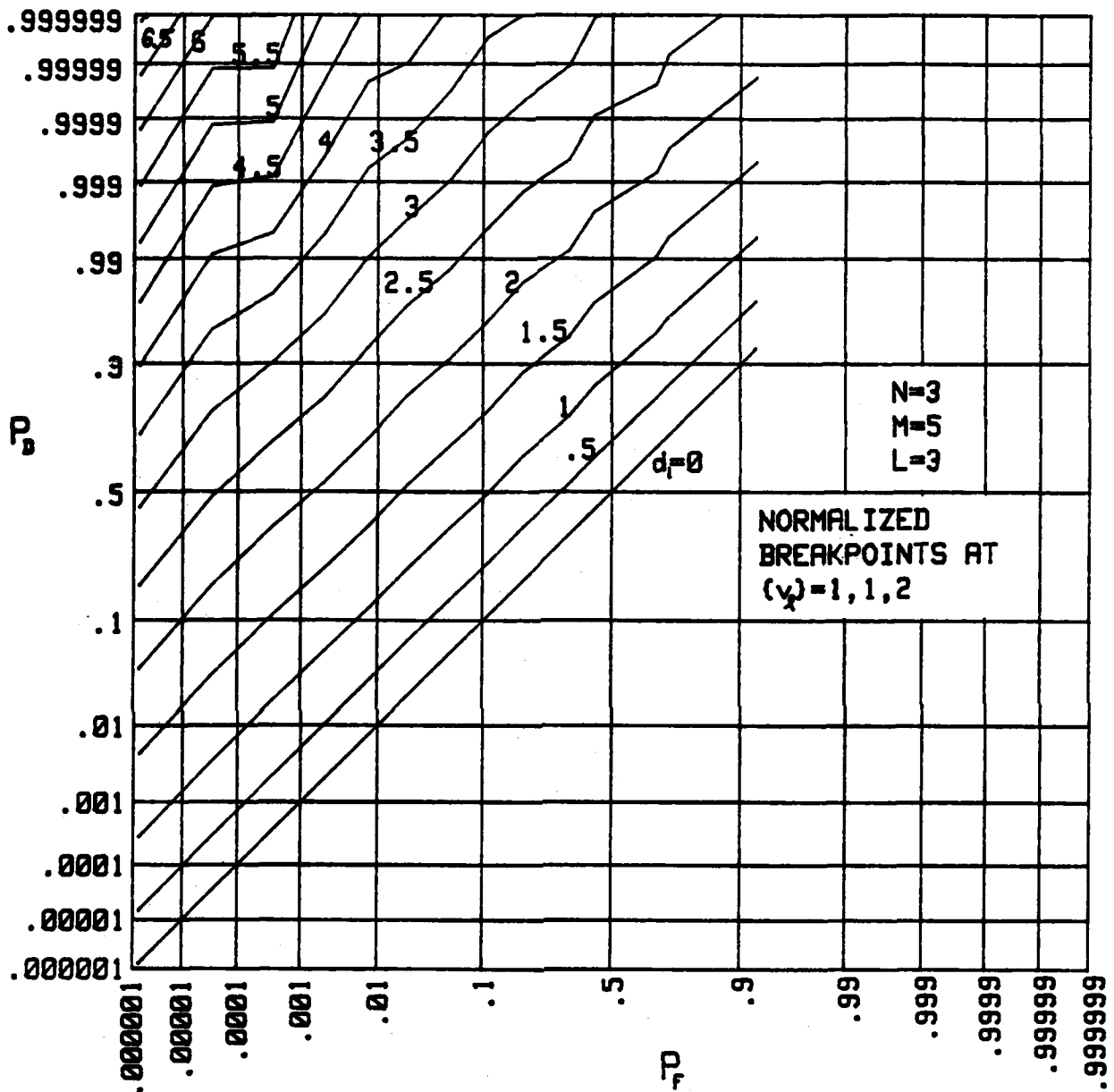
Figure 15. Operating Characteristics for $\{v_\ell\}$ = 1,1,2
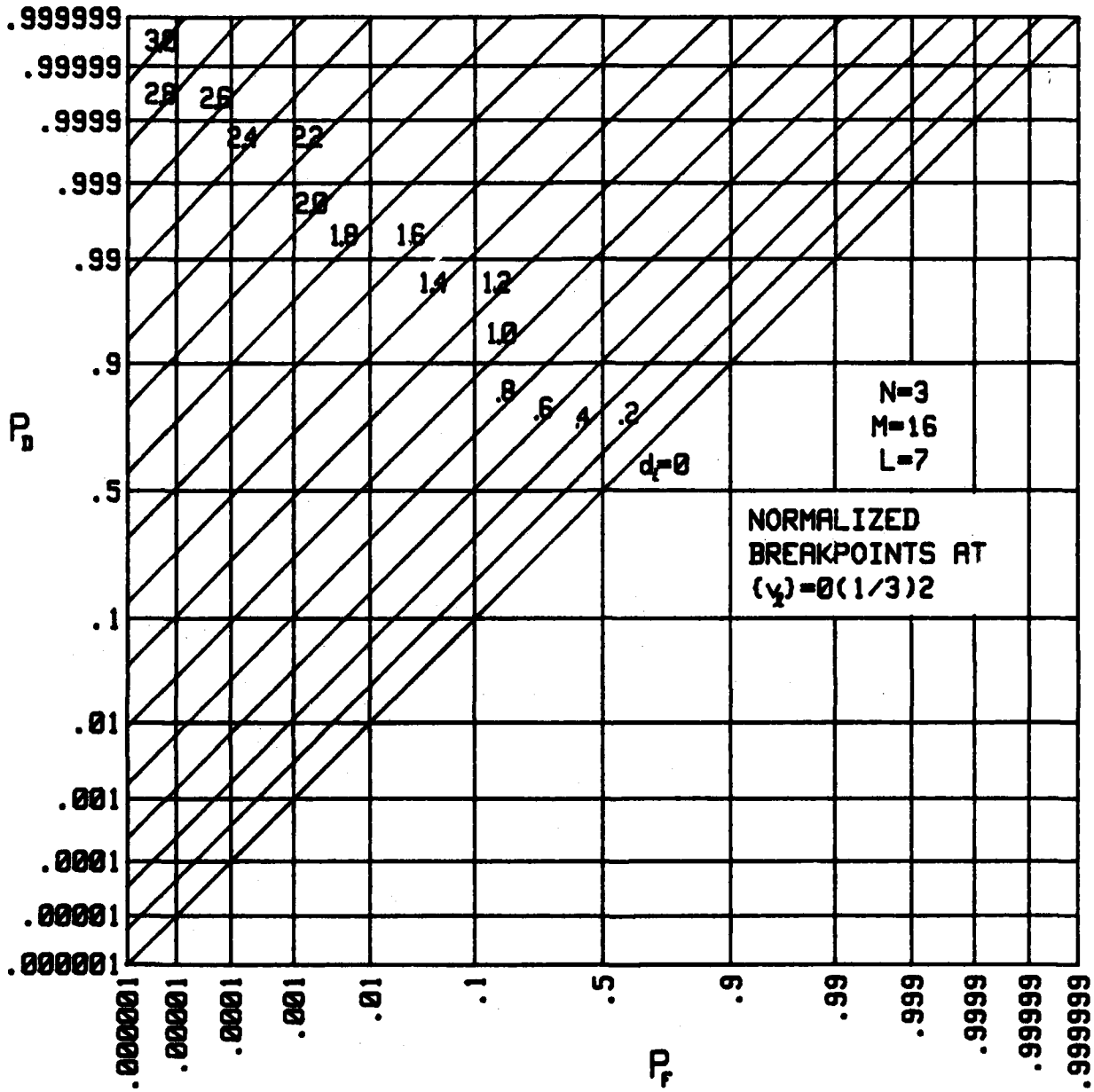
Figure 16. Operating Characteristics for M = 16, $\{v_\ell\}$ = 0(1/3)2
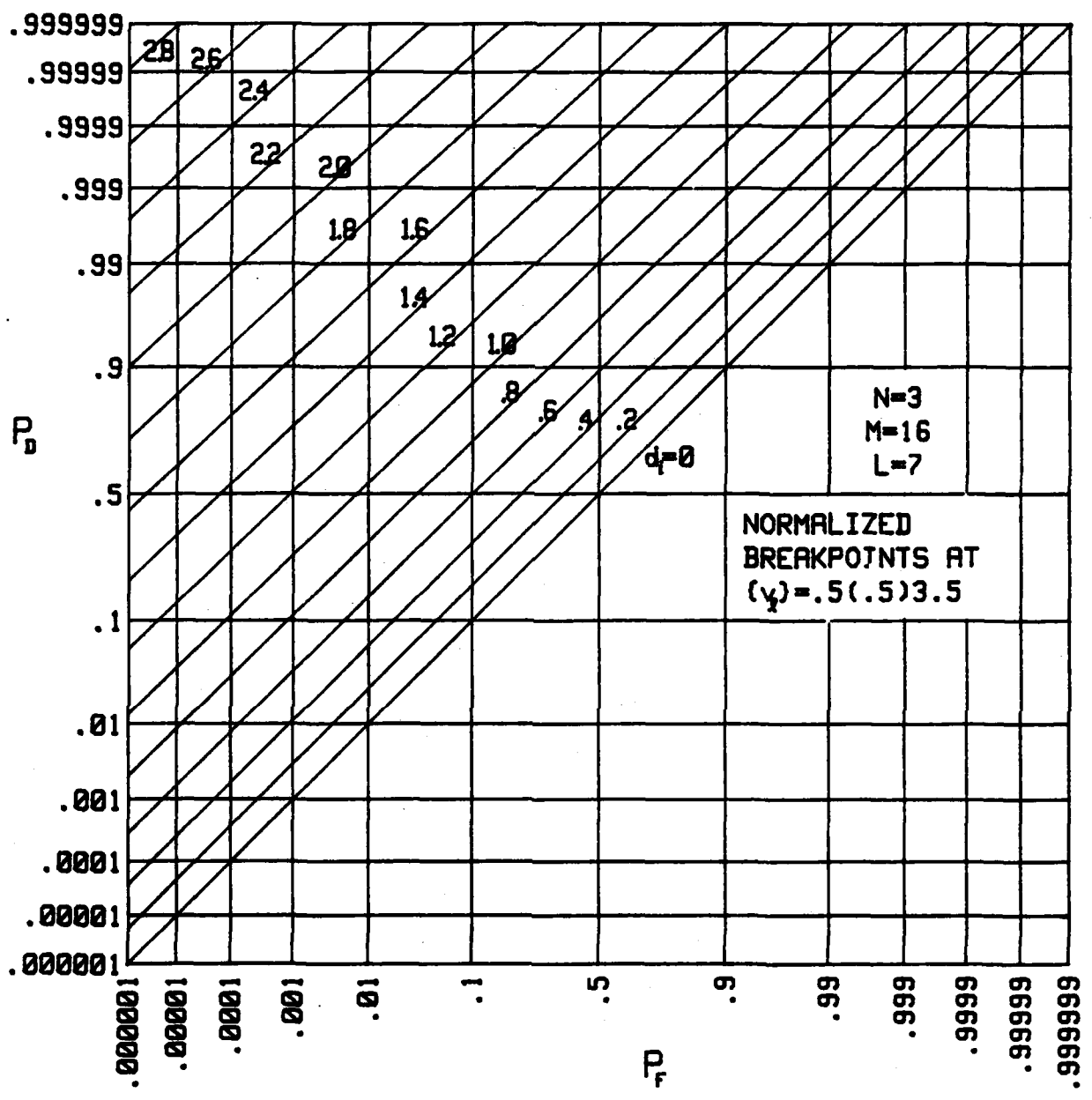
Figure 17. Operating Characteristics for M = 16, $\{v_\ell\}$ = .5(.5)3.5

$$\{y_\ell\} = \begin{cases} 0(1/3)2 & \text{in figure 18} \\ 0(.5)3 & \text{in figure 19} \\ 0(.7)4.2 & \text{in figure 20} \end{cases} . \tag{30}$$

The results in figures 18 through 20 are in almost perfect agreement with the simplified analysis in ref. 2. The normalized breakpoints in figure 19 are best in the intermediate range of detection probabilities; figure 18 is just sligntly better for the high performance region of $d_i = 2.2$.

We now present a series of comparisons where some of the parameters are held constant, while tne remainder are varied in order to determine the effect upon the operating characteristics. The first comparison is for $M=5$, $N=10$, and tne quantizer varied as follows:

$$\begin{cases} L=7, & \{y_\ell\} = 1.4(.45)4.1 & \text{in figure 21} \\ L=3, & \{y_\ell\} = 2(.75)3.5 & \text{in figure 22} \\ L=1, & y_\ell = 2.75 & \text{in figure 23} \end{cases} . \tag{31}$$

These correspond to 3-bit, 2-bit, and 1-bit quantizers respectively, where the normalized breakpoints have been chosen in each case so as to optimize the performance for $d_i = 4$. Increasing L beyond 7, and changing the breakpoints, failed to improve the operating characteristic noticeably above that of figure 21. The increase in the input deflection, d_i, needed to maintain the same performance at $P_F = 1 - P_D \approx 10^{-3.5}$ is approximately 4.5/4 for $L=1$ vs $L=7$. If inputs $\{x_n\}$ are interpreted as voltages, this corresponds approximately to a 1 dB degradation for the hard clipper, $L=1$.

The next series is for $M=5$ and tae quantizer fixed at the 3-bit characteristic in the first line of (31). N is varied over the values 1, 5, 10, 20, 40 in figures 24-28, respectively. The slight improvement in performance, that might ensue from modifying the breakpoints at each N, was not investigated in tnis comparison. Tne effect of increasing N is to degrade the performance, since the or-ing must select one of the input channels for accumulation, and it will not always pick the signal-bearing channel. The increase in d_i required to maintain $P_F = 1 - P_D \approx 10^{-5}$ is approximately $5.25/4 = 2.35$ dB for $N=40$ vs $N=1$.
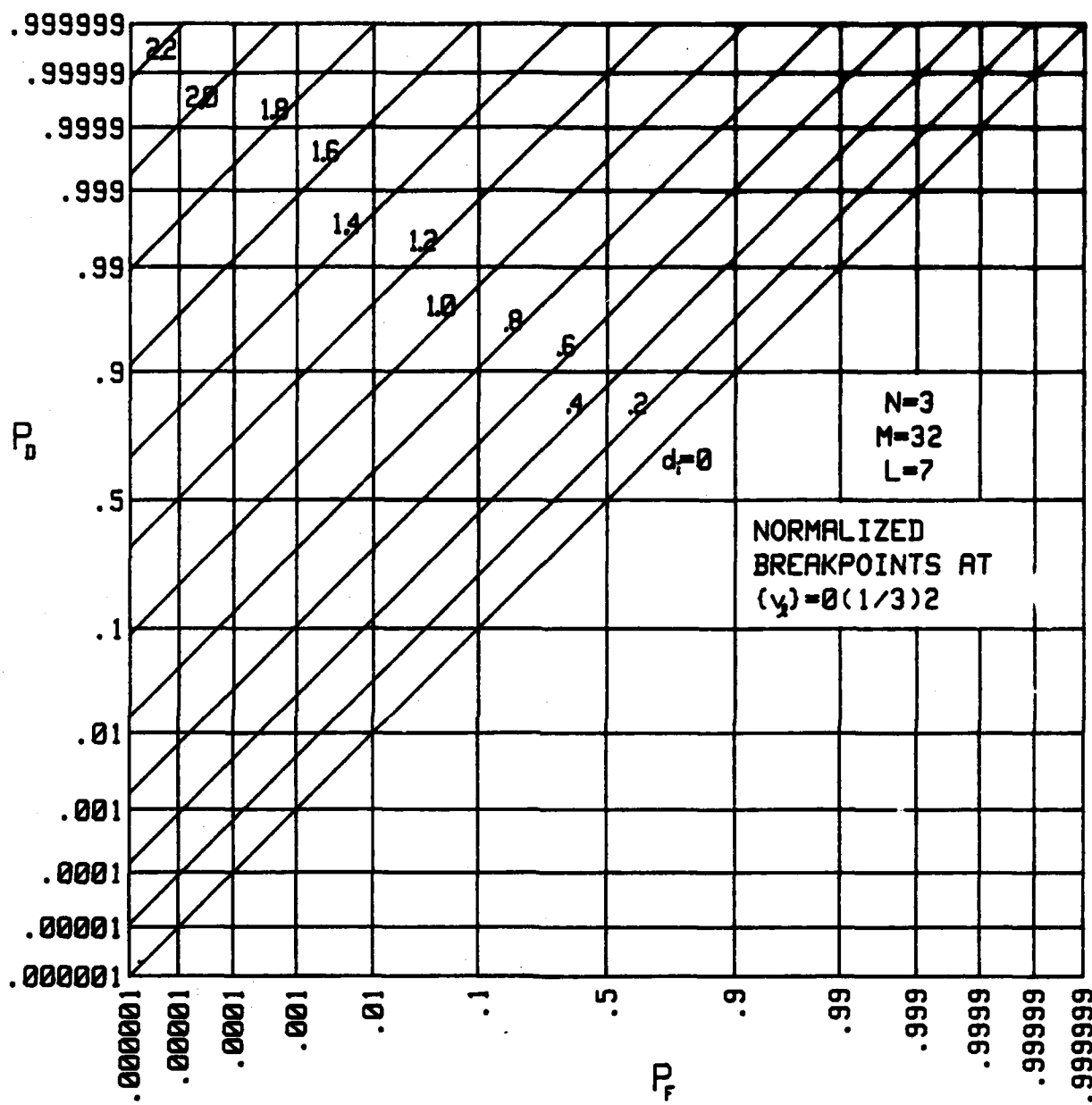
Figure 18. Operating Characteristics for M = 32, $\{v_\ell\}$ = 0(1/3)2
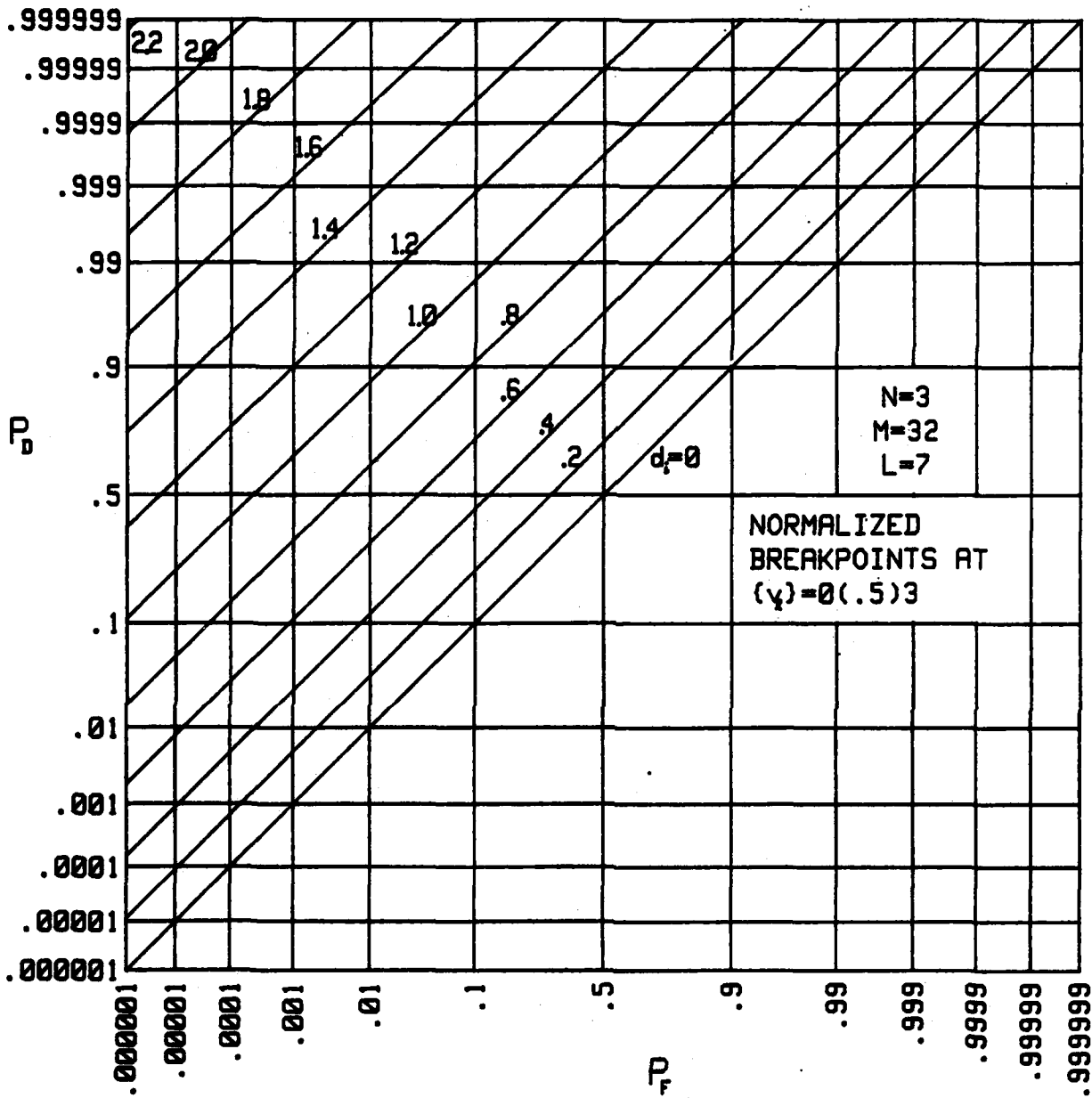
Figure 19.   Operating Characteristics for M = 32, $\{v_\ell\}$ = 0(.5)3
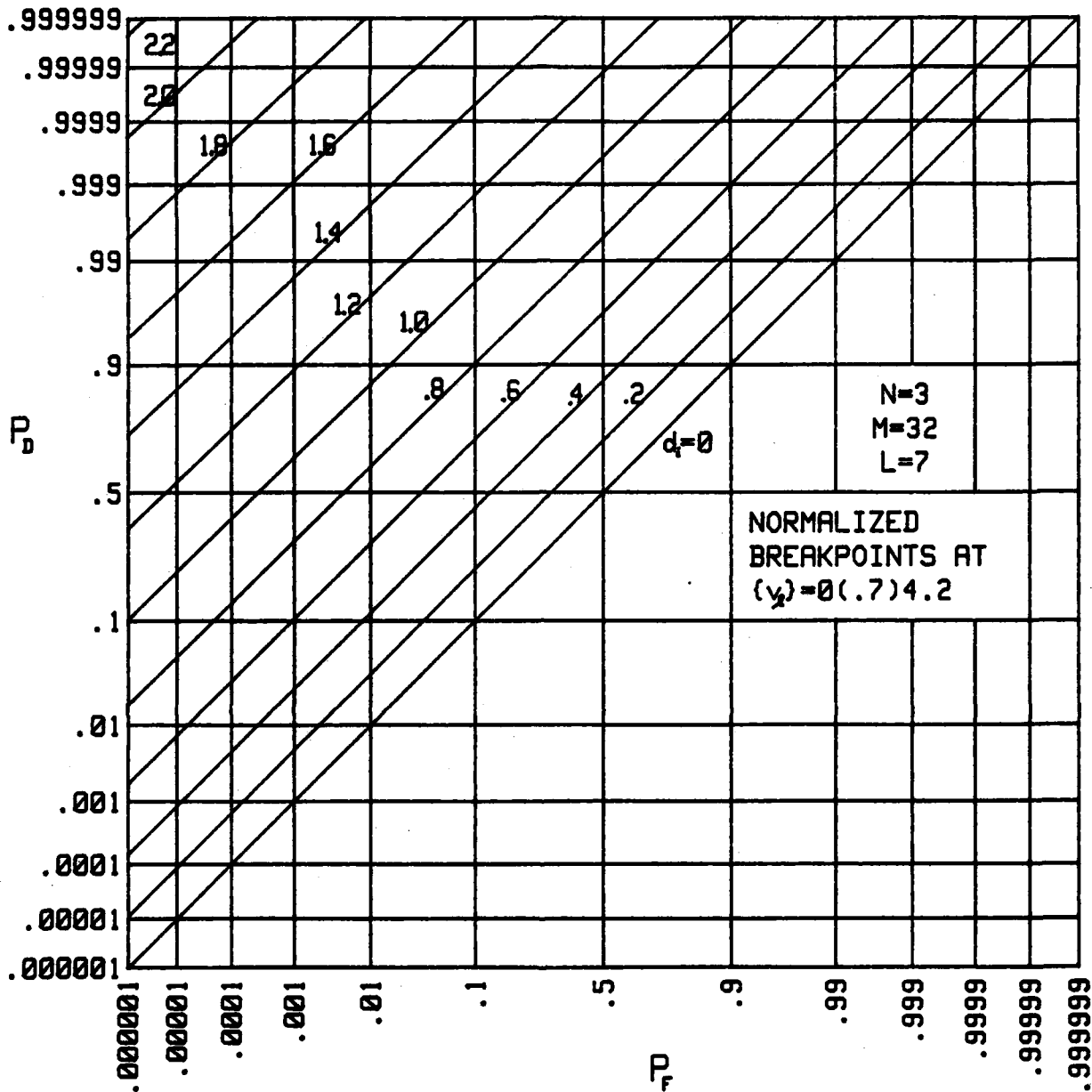
Figure 20. Operating Characteristics for M = 32, $\{v_\ell\}$ = 0(.7)4.2
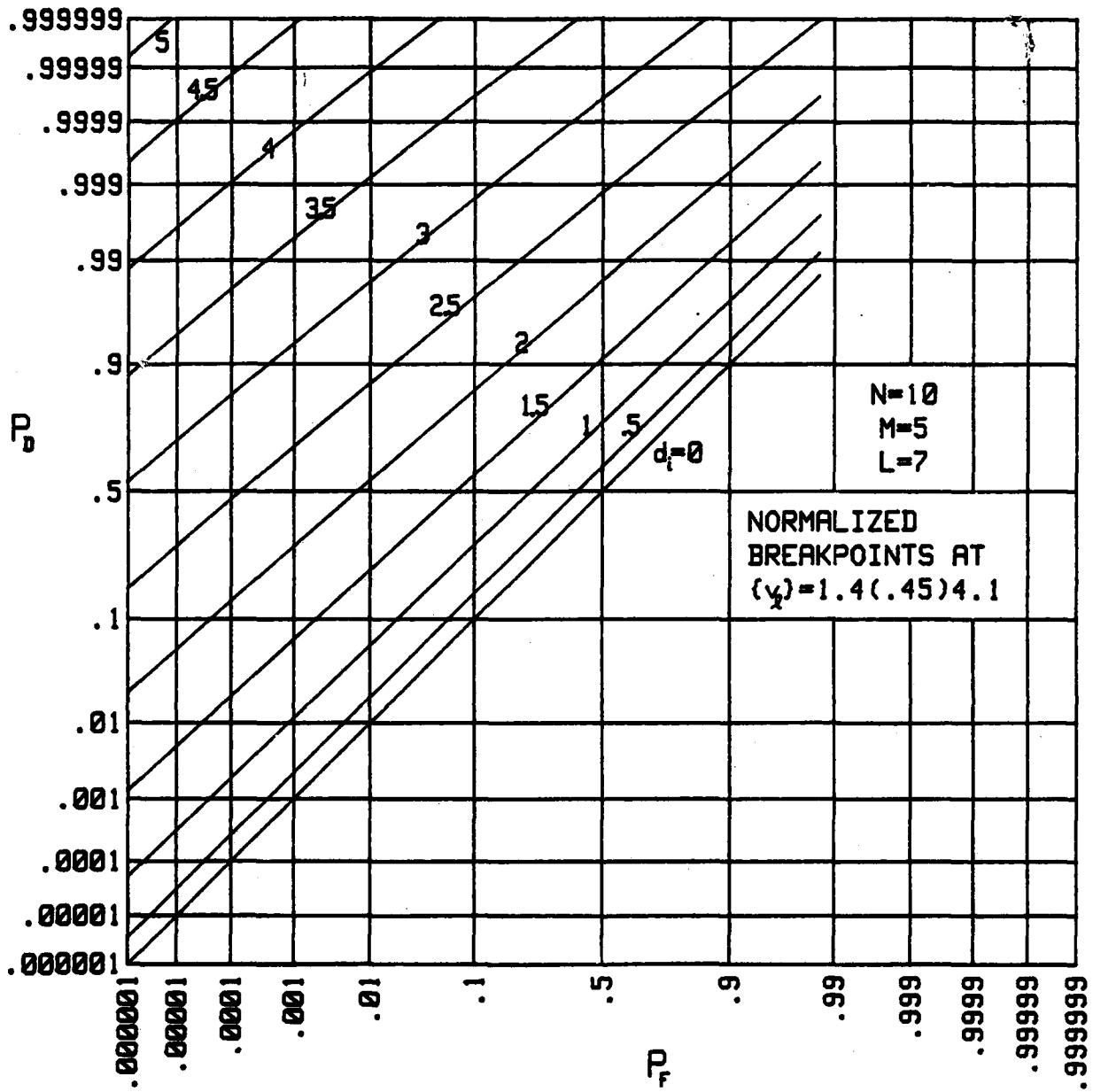
Figure 21. Operating Characteristics for L = 7
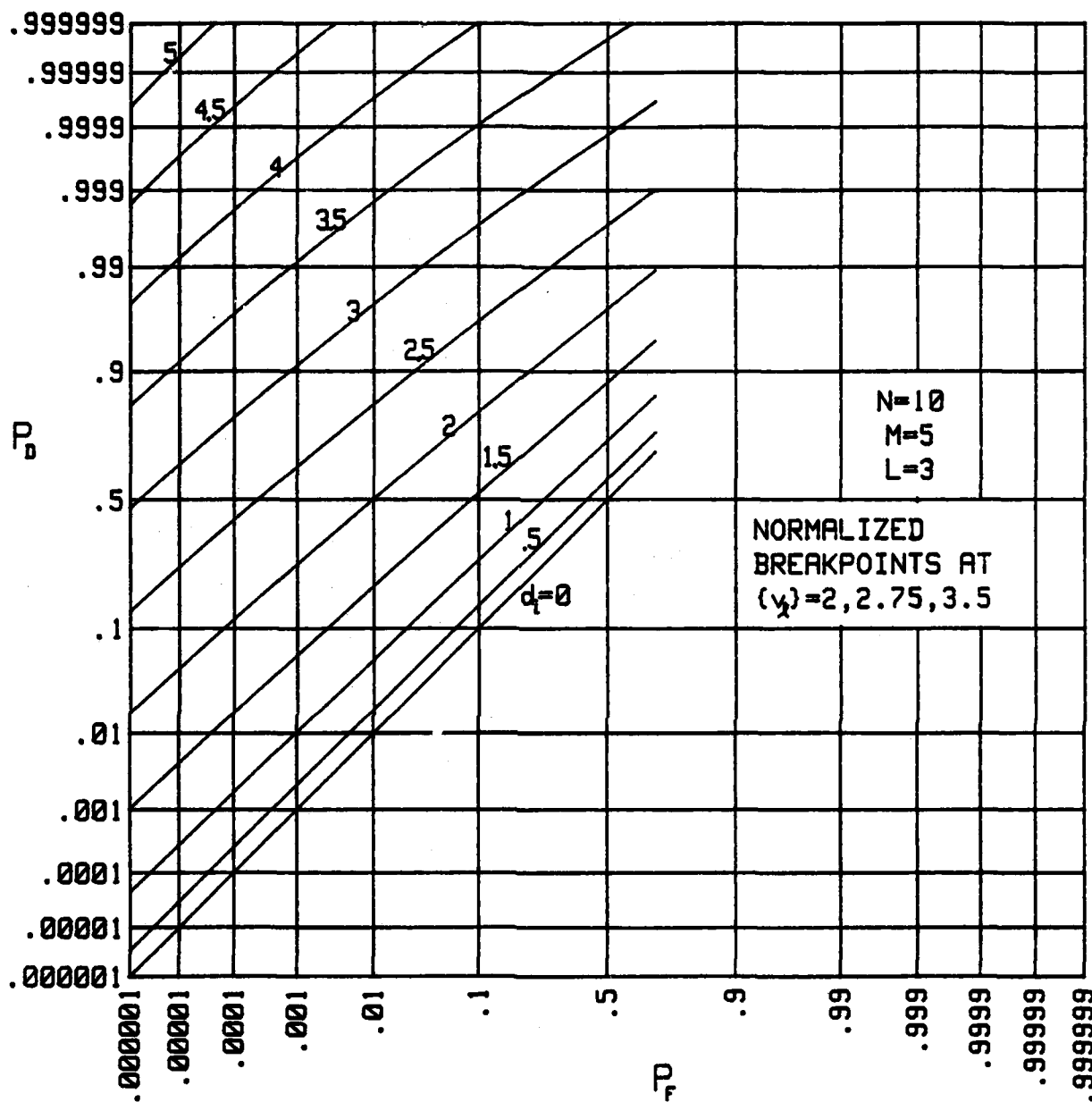
Figure 22. Operating Characteristics for L = 3
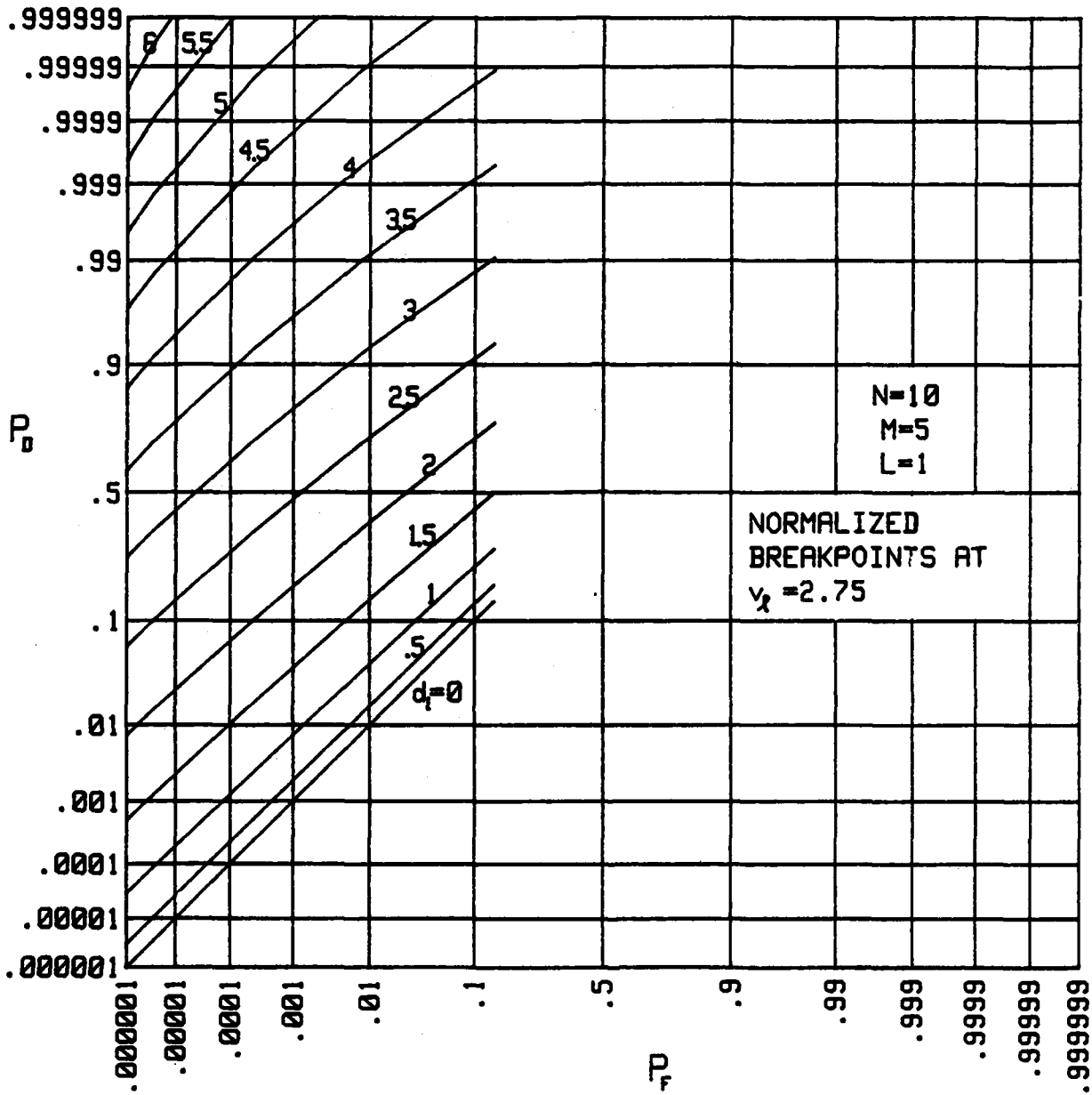
Figure 23. Operating Characteristics for L = 1
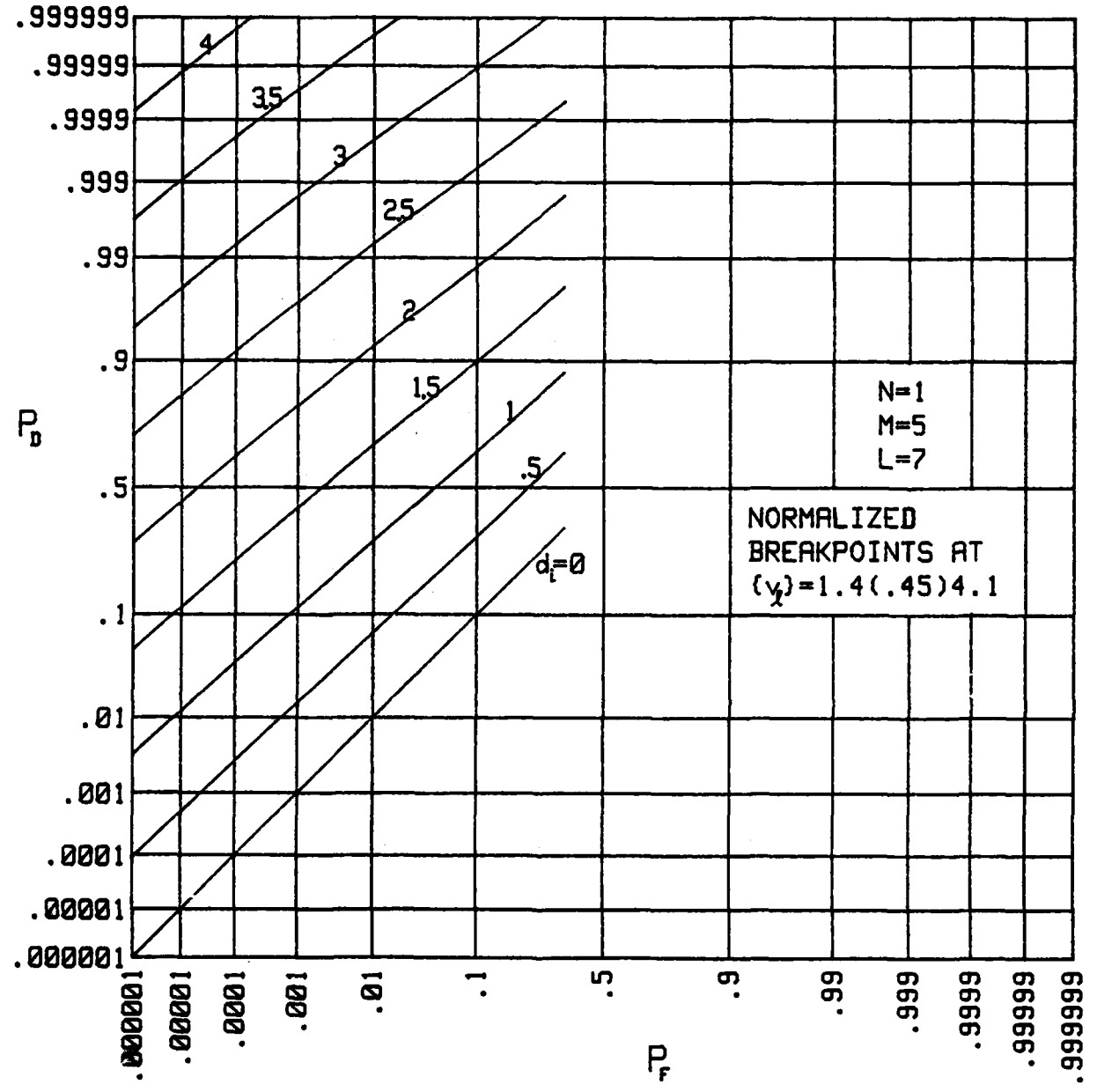
Figure 24. Operating Characteristics for N = 1
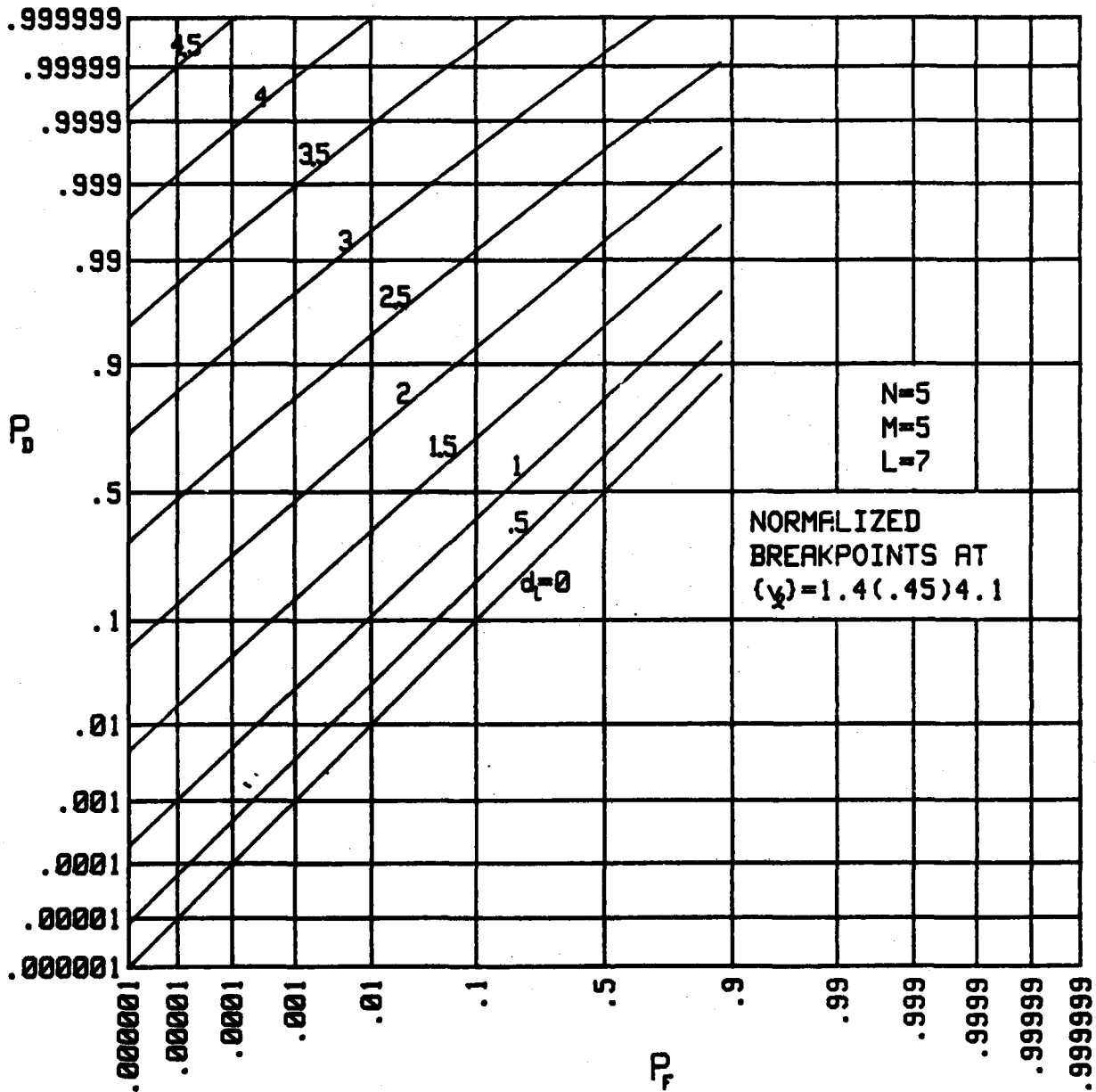
Figure 25. Operating Characteristics for N = 5
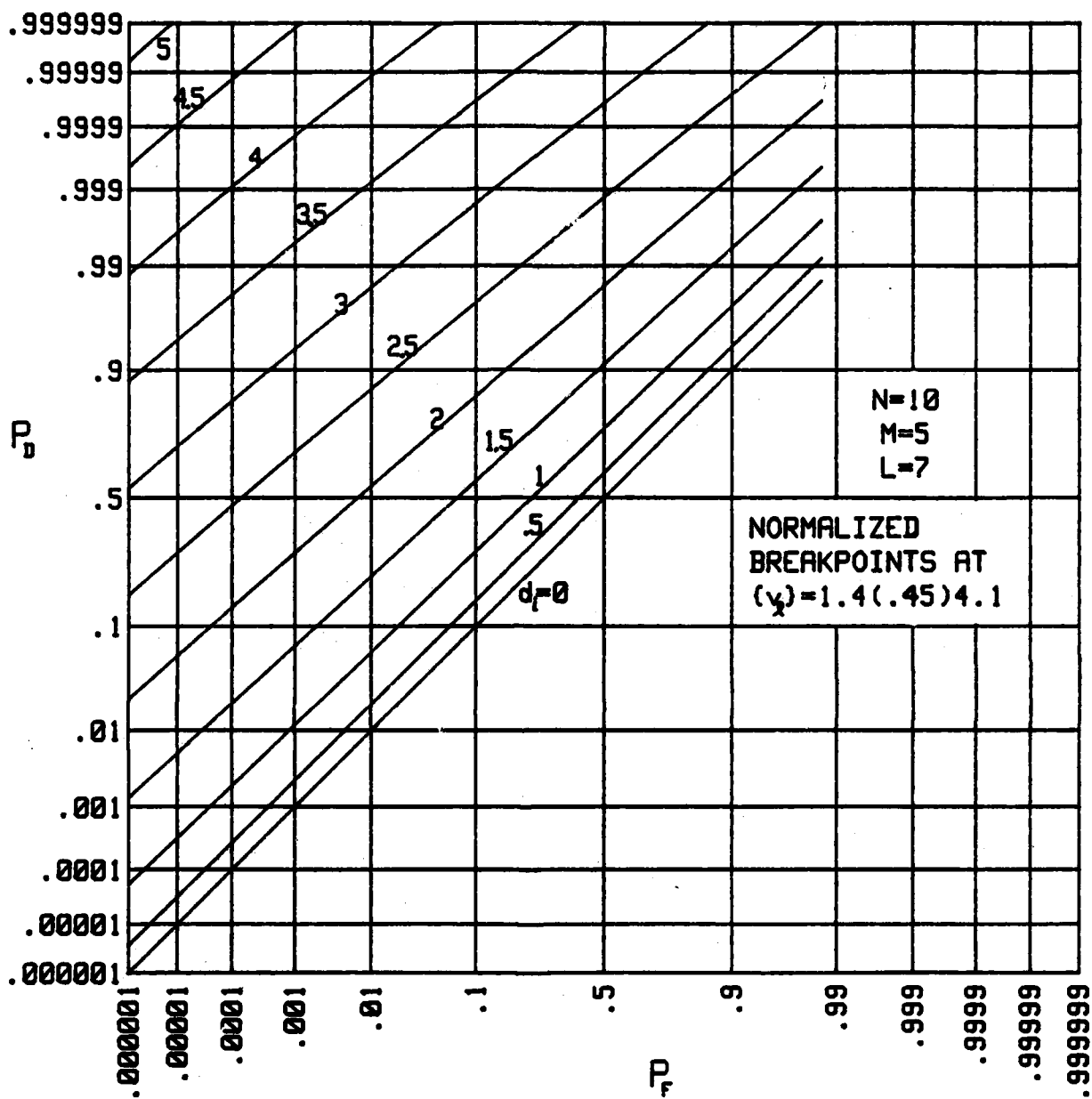
Figure 26.   Operating Characteristics for N = 10
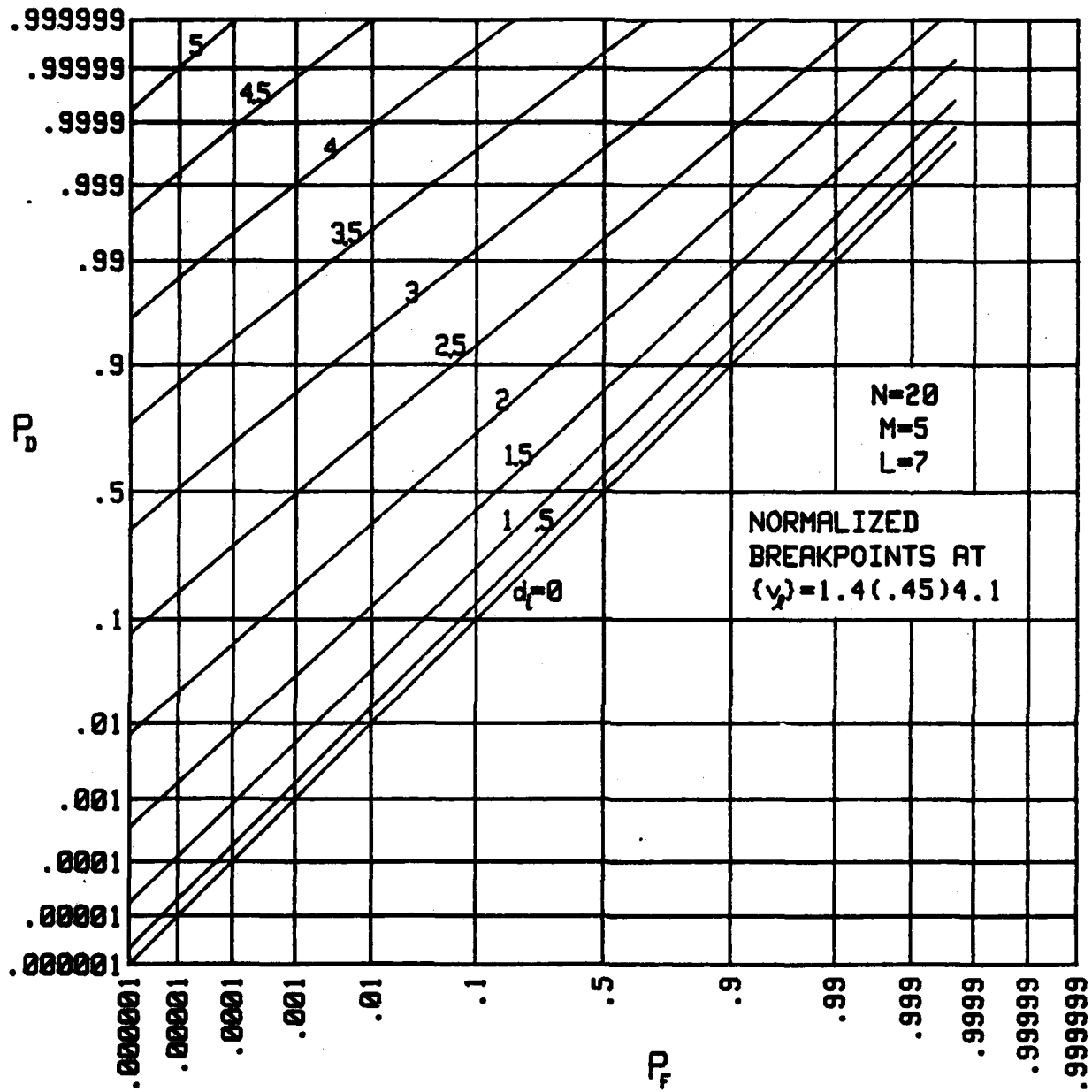
Figure 27. Operating Characteristics for N = 20
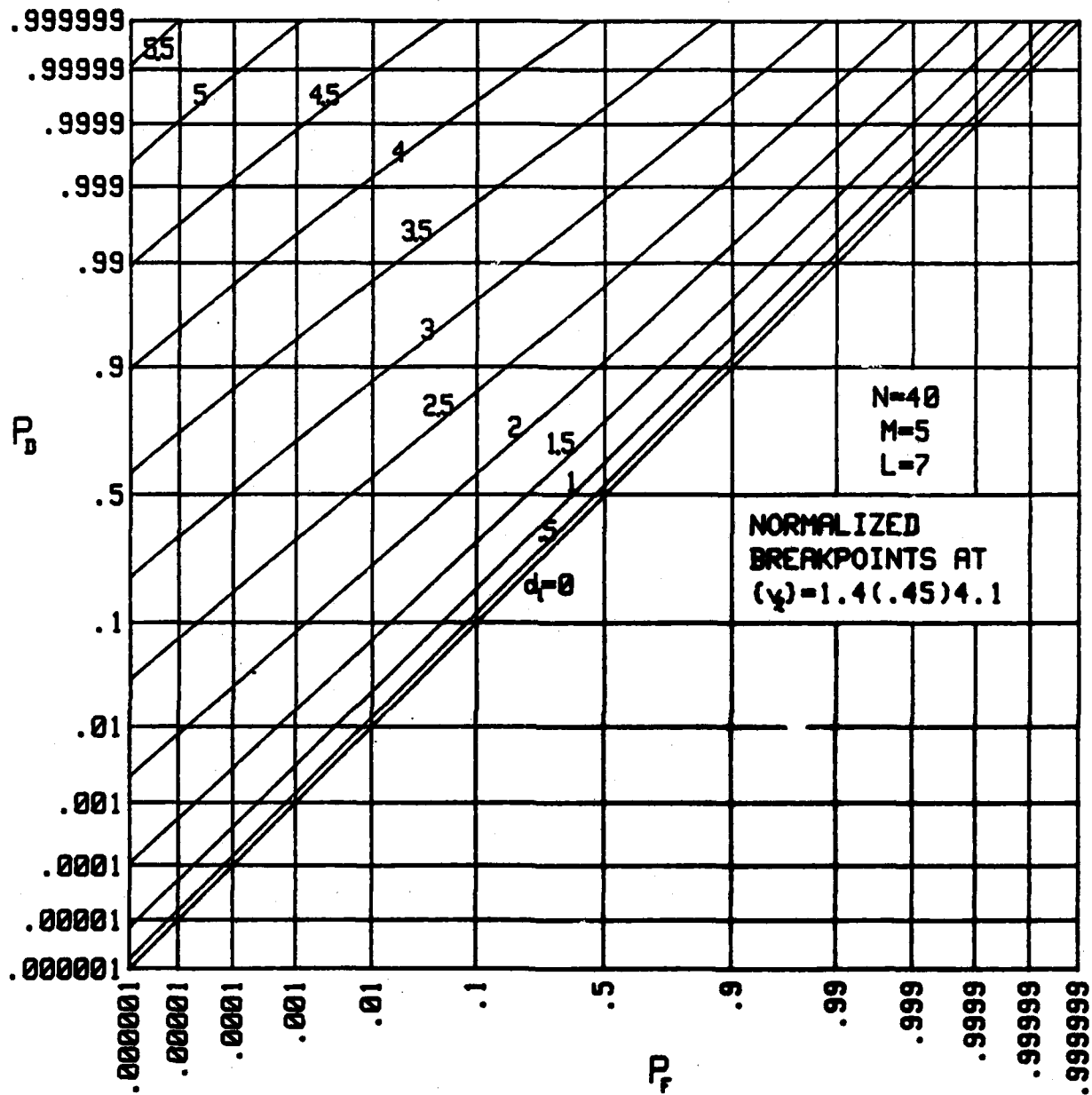
Figure 28. Operating Characteristics for N = 40

The last series investigates the effect of varying M. In figures 29 through 33, M takes on the values 1, 2, 5, 10, and 20, respectively. The effect of increasing M is to realize better performance with smaller input signal-to-noise ratios. The decrease in d_i allowed, in order to maintain $P_F = 1 - P_D \approx 10^{-3}$, is approximately $2.4/6.8 = -9$ dB for M=20 vs M=1. When M is made large, the approximate analysis in ref. 2 can be used with confidence; this is fortunate, since in the case of very large M, the DFT size, $N_f \geq ML+1$, required here may not be easily attainable on some computer setups.
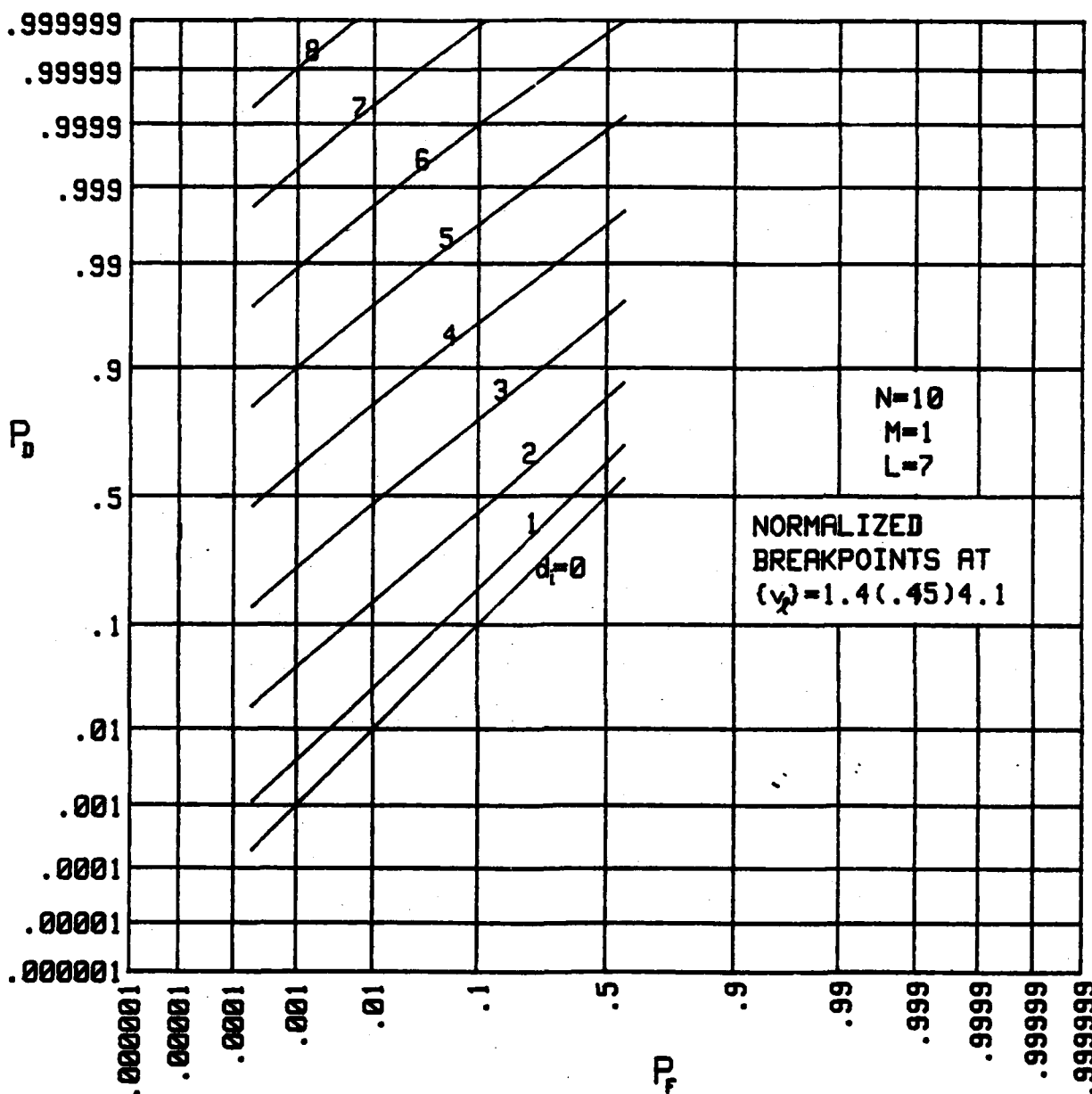
Figure 29.   Operating Characteristics for M = 1
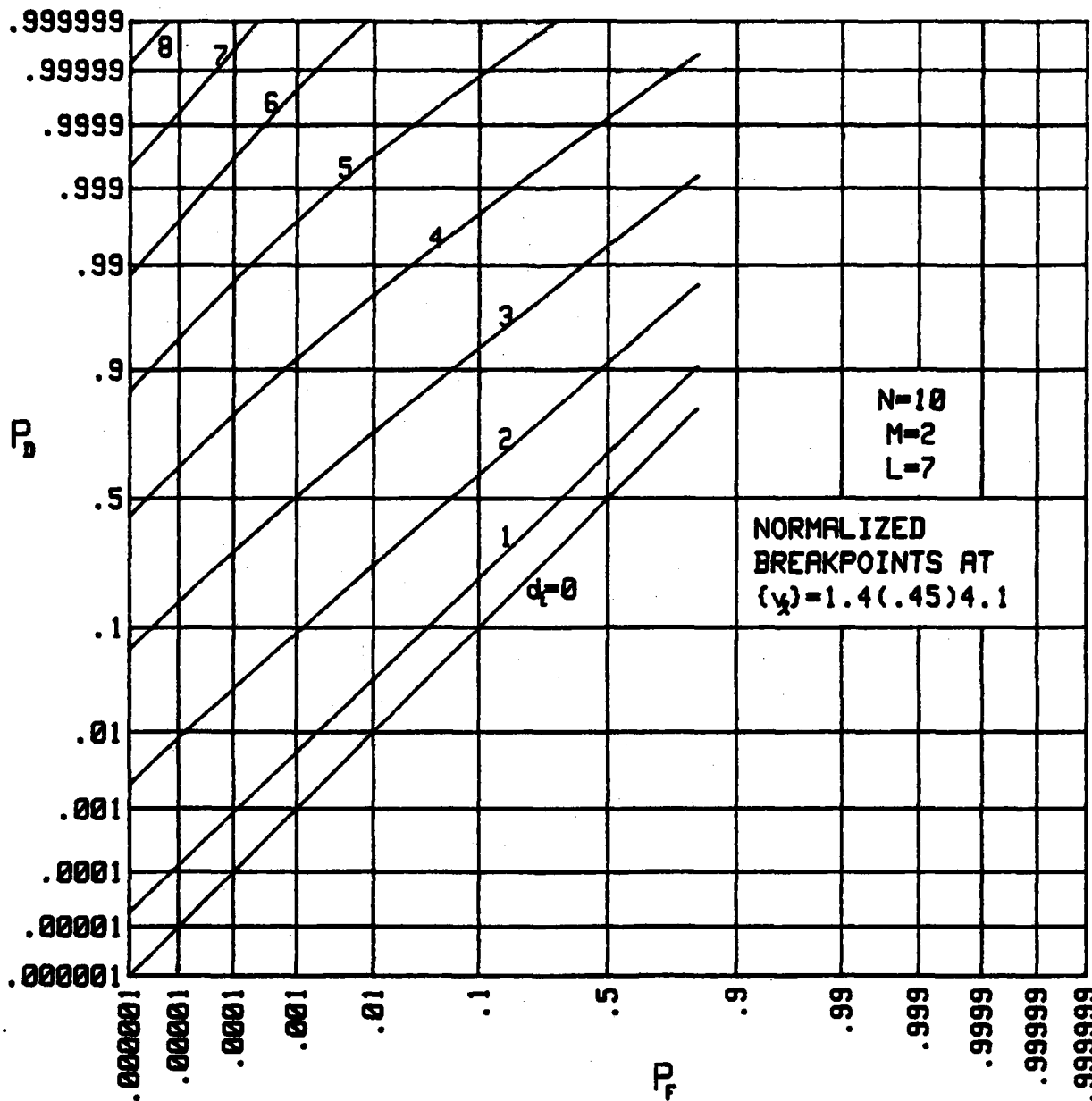
Figure 30.   Operating Characteristics for M = 2
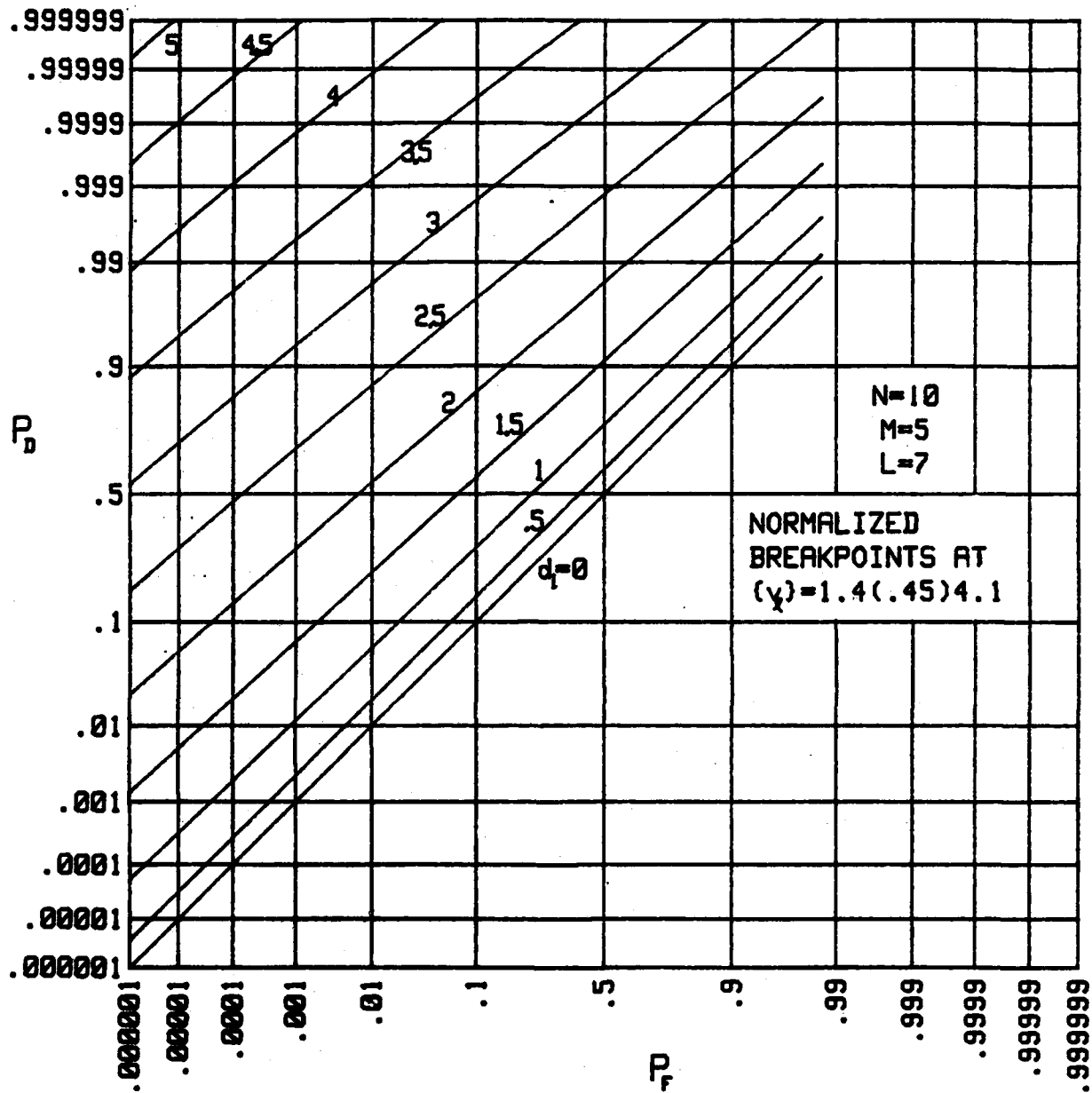
Figure 31. Operating Characteristics for M = 5
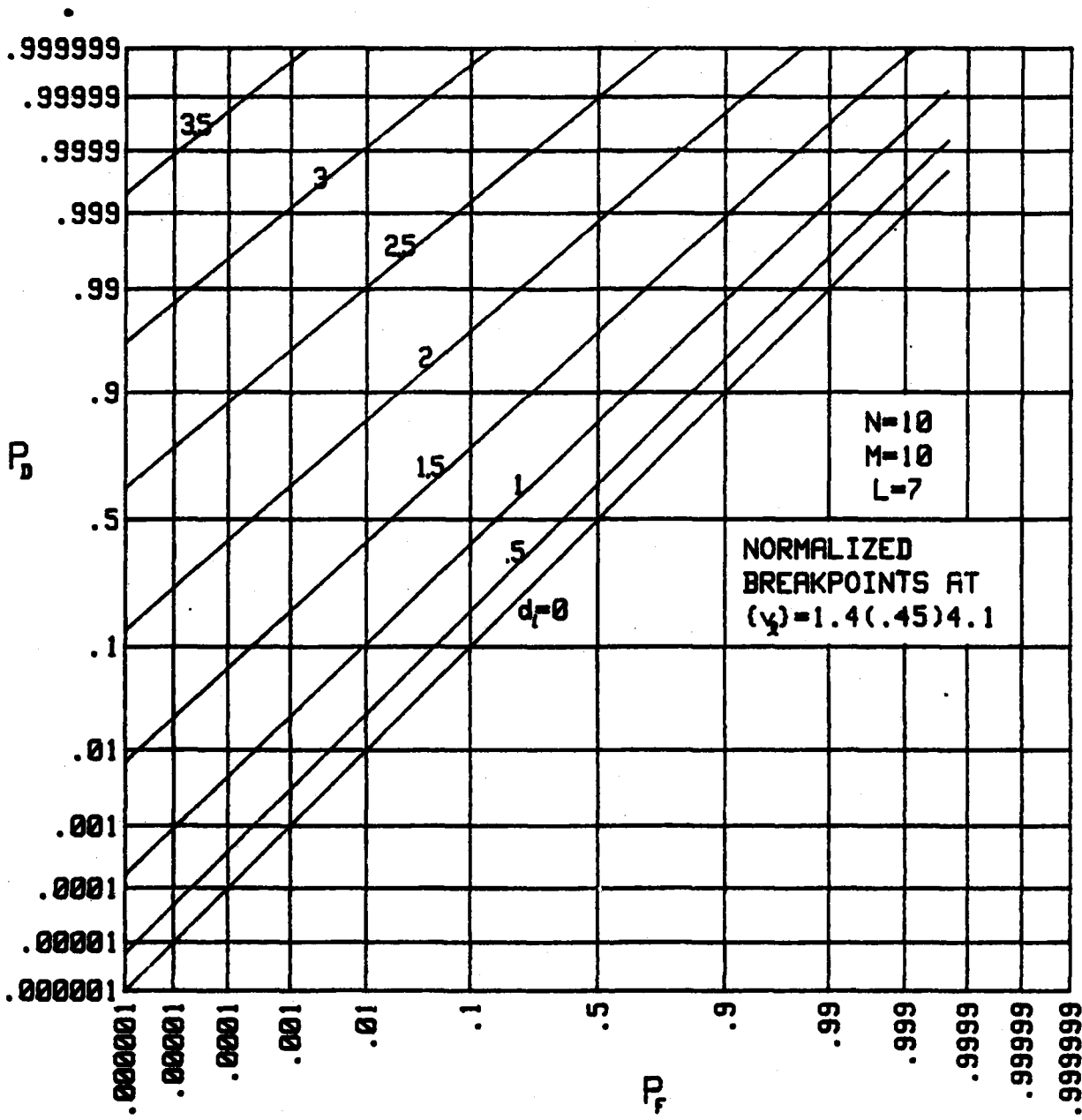
Figure 32.   Operating Characteristics for M = 10
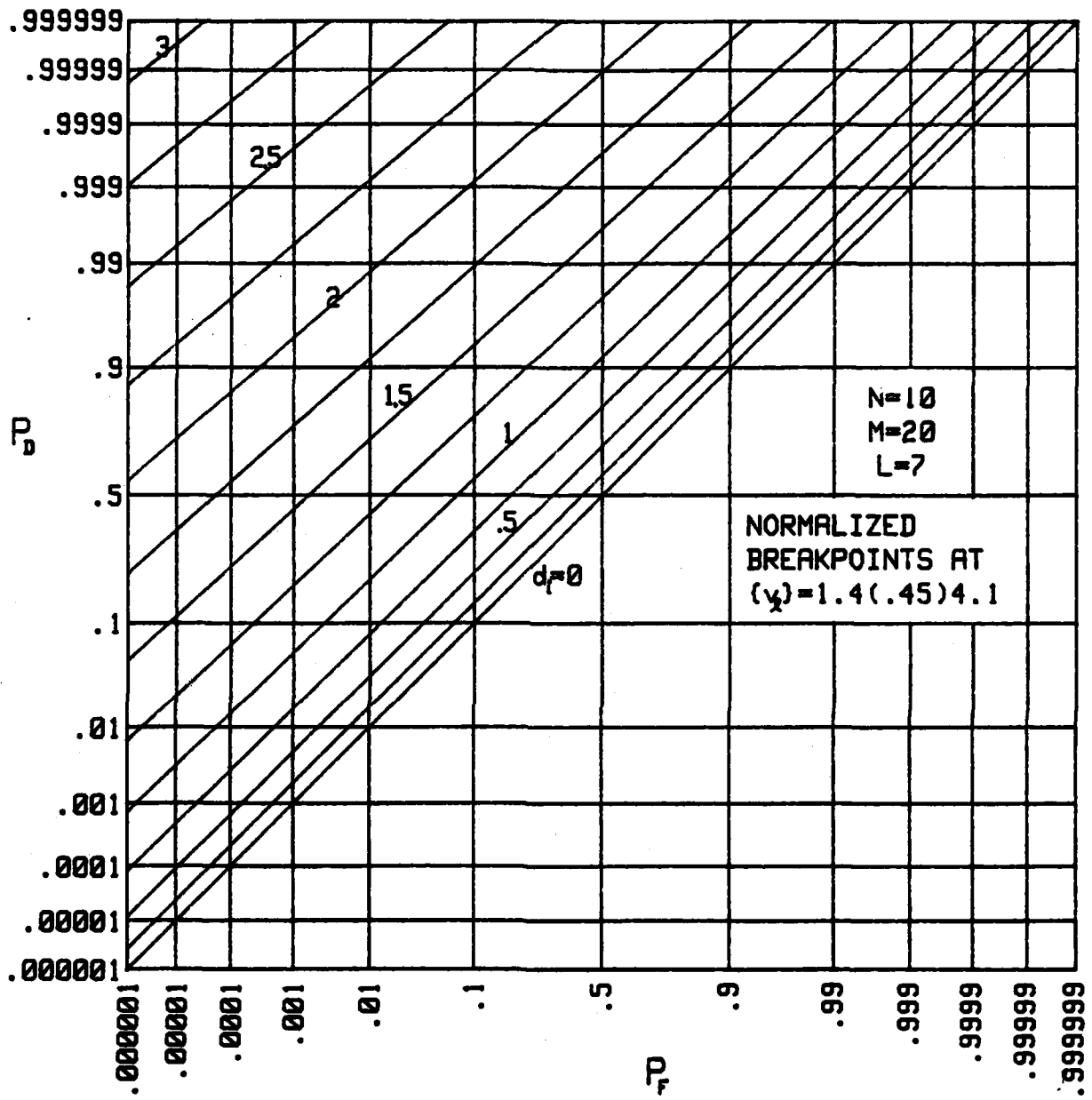
Figure 33. Operating Characteristics for M = 20

DISCUSSION

Tne large number of possible combinations of values of N, M, L, and $\{y_i\}_1^L$ precludes an exhaustive compilation of results. Instead we have presented some representative examples and give a program in appendix C by which the user can investigate his particular situation and alternatives. This program gives exact results for any quantizer, provided only that ML is not too large and that round-off errors do not get out of hand. For extremely large M, a Gaussian approximation for the decision variable is justified and the analysis of ref. 2 is applicable.

If tne quantizer is not specialized to the equal ordinate spacings of figure 3, but is of the general form depicted in figure 2, the performance analysis is more difficult. However, the characteristic function of the decision variable is still capable of a closed form expression; see appendix D. Evaluation of tne cumulative distribution function of the decision variable is possible via one FFT, according to the methods given in refs. 6 and 7. No numerical investigation nas been undertaken of this case.

In appendix E, the form of the optimum processor operating on N input channels, of whicn only one may contain a signal, is derived and then specialized to the Gaussian input example of (16). This optimum processor, in general, requires knowledge of the absolute levels of the input signal and noise. However, for $d_i > 2$, the form of the optimum processor approaches that of figures 1 or 5, where the quantizer is replaced by a linear device, and tne aosolute level knowledge is no longer required. Thus the performance of the system considered here should be nearly optimum for large L and well-placed oreakpoints.

Exact analysis of the system of figures 1 or 5, with a linear gain instead of a quantizer, is _more_ difficult than that given here. A simplified second-moment analysis was presented in ref. 1; an exact analysis is possible and will be presented by the author in a future report.

A detailed comparison of the exact performance results obtainable via this report, with the second-moment results given in refs. 1-5, has revealed excellent agreement over a wide range of parameter values. However, until an extensive thorough investigation of the two approaches is made for a wide range of values of N, M, L, $\{v_\ell\}$, P_F, and P_D, it is difficult to state exactly where the earlier approximate analyses can be used with full confidence. This time-consuming investigation has not been undertaken; however, the program in appendix C affords the mechanism whereby this comparison can be conducted. The statements here regarding large M and moderate P_F can only be made quantitative after this study is completed.

·

Appendix A

INTERRELATIONS BETWEEN CHARACTERISTIC FUNCTIONS AND
PROBABILITY DENSITY FUNCTIONS OF DISCRETE RANDOM VARIABLES

Suppose random variable x is limited to the integer values 0, 1, ..., N, and that the probability of taking on value n is a_n. That is, the probability density function of x is

$$p_x(u) = \sum_{n=0}^{N} a_n \, \delta(u-n) \quad .$$

(A-1)

The characterisic function of x is then

$$f_x(\xi) = \int_{-\infty}^{\infty} du \, \exp(i\xi u) \, p_x(u) = \sum_{n=0}^{N} a_n \, \exp(i\xi n) \quad ;$$

(A-2)

this function has period 2π in ξ.

Now let integer M be selected such that

$$M \geq N+1 \quad .$$

(A-3)

Tnen consider M samples of characteristic function f_x at increment $2\pi/M$; that is, consider the set of samples

$$f_x(m2\pi/M) \quad \text{for } 0 \leq m \leq M-1 \quad .$$

(A-4)

Now let us take an M-point DFT of these samples, and scale by 1/M; that is, for $0 \leq k \leq M-1$,

$$\frac{1}{M} \sum_{m=0}^{M-1} \exp(-i2\pi mk/M) f_x(m2\pi/M)$$

$$= \frac{1}{M} \sum_{m=0}^{M-1} \exp(-i2\pi mk/M) \sum_{n=0}^{N} a_n \exp(i2\pi nm/M)$$

$$= \sum_{n=0}^{N} a_n \frac{1}{M} \sum_{m=0}^{M-1} \exp(i2\pi(n-k)m/M)$$

$$= \sum_{n=0}^{N} a_n \delta_{n-k}^{(M)} = \begin{Bmatrix} a_k & \text{for } 0 \le k \le N \\ 0 & \text{for } N < k \le M-1 \end{Bmatrix} . \tag{A-5}$$

Here, in the second line, we used expression (A-2) for the characteristic function, and in the last line, we used (A-3).

Expression (A-5) states that the scaled M-point DFT of the set of characteristic function samples, (A-4), yields precisely the areas $\{a_k\}_0^N$ of the impulses in probability density function p_x, provided that $M \ge N+1$. The values returned by the DFT for $a_{N+1}, \ldots, a_{M-1}$ should all be zero.

More generally, if random variable x is limited to the values

$$h_0, \; h_0 + \Delta h, \; \ldots, \; h_0 + N \, \Delta h, \tag{A-6}$$

the characteristic function takes the form

$$f_x(\xi) = \exp(i\xi h_0) \sum_{n=0}^{N} a_n \exp(i\xi n \, \Delta h) \quad . \tag{A-7}$$

In this case, the sample set that must be subjected to an M-point DFT is not (A-4), but rather

$$f_x\left(\frac{2\pi m}{M\Delta h}\right) \exp\left(-i \, \frac{2\pi m}{M\Delta h} \, h_0\right) \quad \text{for } 0 \le m \le M-1 \quad . \tag{A-8}$$

When scaled by 1/M, this DFT yields areas $\{a_n\}$ directly.

Appendix B

ALTERNATIVE INPUT STATISTICS

Here we give the equations for two other typical random processes that could serve as candidates for inputs to the nonlinear system of interest. No numerical results have been evaluated for either of the following.

CHI-SQUARED RANDOM VARIABLES

This case could correspond to Gaussian noise with additive Gaussian signal, after passage through a square-law device and summation. That is, under H_1, consider the signal-bearing channel input to be the sum

$$x(m) = \sum_{k=1}^{2D} \left[s_k(m) + n_k(m) \right]^2 \quad , \tag{B-1}$$

where $\{s_k(m)\}$ and $\{n_k(m)\}$ are independent zero-mean Gaussian random variables with variances σ_s^2 and σ_n^2 for the signal and noise, respectively. x is a Chi-squared variate with $2D$ degrees of freedom.

Letting $\sigma_1^2 = \sigma_s^2 + \sigma_n^2$, the probability density function of x is given by

$$p_x^{(1)}(u) = \frac{u^{D-1}}{(D-1)! \left(2\sigma_1^2\right)^D} \exp\left(-\frac{u}{2\sigma_1^2}\right) \quad \text{for } u > 0 \quad . \tag{B-2}$$

The cumulative distribution function of x is, via repeated integration by parts, given by

$$P_x^{(1)}(u) = 1 - \exp\left(-\frac{u}{2\sigma_1^2}\right) e_{D-1}\left(\frac{u}{2\sigma_1^2}\right) \quad \text{for } u > 0 \quad , \tag{B-3}$$

where (ref. 8, 6.5.11)

$$e_{D-1}(t) = \sum_{n=0}^{D-1} \frac{1}{n!} t^n \tag{B-4}$$

is the first D terms of exp(t).

The cumulative distribution function of x under H_0 follows immediately from (B-3) by setting $\sigma_s^2 = 0$ and identifying $\sigma_0^2 = \sigma_n^2$:

$$P_x^{(0)}(u) = 1 - \exp\left(-\frac{u}{2\sigma_0^2}\right) e_{D-1}\left(\frac{u}{2\sigma_0^2}\right) \quad \text{for } u > 0 \quad . \qquad (B-5)$$

In fact, (B-3) and (B-5) could be used as input statistics for the analysis contained here in the main body of the report, without the need for interpretation (B-1); (B-1) merely lends the physical interpretation of x as the sum of a number of diversity inputs.

According to (5) and (6), we need the quantities

$$\left. \begin{array}{l} P_x^{(0)}(b_\ell) = 1 - \exp(-y_\ell)\, e_{D-1}(y_\ell) \\ \\ P_x^{(1)}(b_\ell) = 1 - \exp\left(-\frac{\sigma_0^2}{\sigma_1^2}y_\ell\right) e_{D-1}\left(\frac{\sigma_0^2}{\sigma_1^2}y_\ell\right) \end{array} \right\} \text{for } 1 \le \ell \le L \quad , \qquad (B-6)$$

where now the normalized breakpoints are defined as

$$y_\ell = \frac{b_\ell}{2\sigma_0^2} \quad \text{for } 1 \le \ell \le L \quad . \qquad (B-7)$$

Of course, we should always select $b_\ell \ge 0$, since x is never negative.

NONCENTRAL CHI-SQUARED RANDOM VARIABLES

This case corresponds to Gaussian noise with additive deterministic signal, after passage through a squarer and summation. Under H_1, let the input be composed as follows:

$$x(m) = \sum_{k=1}^{20}\left[c_k(m) + n_k(m)\right]^2 \quad , \qquad (B-8)$$

where $\{c_k(m)\}$ are constants, and noises $\{n_k(m)\}$ are independent zero-mean Gaussian random variables with variance σ_n^2. For example, x(m) corresponds to

the sum of D squared-envelopes of the output of a narrowband filter subjected to a sinewave and Gaussian noise. Tne probability density function of x in (B-8) is

$$p_x^{(1)}(u) = \frac{1}{2\sigma_n^2} \left(\frac{\sqrt{u}}{a\sigma_n}\right)^{D-1} \exp\left(-\frac{a^2}{2} - \frac{u}{2\sigma_n^2}\right) I_{D-1}\left(\frac{a\sqrt{u}}{\sigma_n}\right) \quad \text{for } u > 0, \qquad (B-9)$$

where

$$a \equiv \frac{1}{\sigma_n} \left[\sum_{k=1}^{2D} c_k^2(m)\right]^{1/2} \qquad (B-10)$$

is a measure of the total signal-to-noise ratio of random variable $x(m)$. (a is generally a function of m.) The cumulative distribution function is

$$P_x^{(1)}(u) = 1 - Q_D\left(a, \frac{\sqrt{u}}{\sigma_n}\right) \quad \text{for } u > 0 \quad , \qquad (B-11)$$

where the Q-function is (ref. 9)

$$Q_D(a,b) \equiv \int_b^\infty dt \, t\left(\frac{t}{a}\right)^{D-1} \exp\left(-\frac{t^2 + a^2}{2}\right) I_{D-1}(at) \quad . \qquad (B-12)$$

Tne probability density function and cumulative distribution function under H_0 follow from (B-9) and (B-11) by setting $a=0$, where we presume that $\{c_k(m)\}$ represent the signal components in (B-8); there results

$$p_x^{(0)}(u) = \frac{u^{D-1}}{(D-1)! \left(2\sigma_n^2\right)^D} \exp\left(-\frac{u}{2\sigma_n^2}\right) \quad \text{for } u > 0 \qquad (B-13)$$

and

$$P_x^{(0)}(u) = 1 - \exp\left(-\frac{u}{2\sigma_n^2}\right) e_{D-1}\left(\frac{u}{2\sigma_n^2}\right) \quad \text{for } u > 0 \quad . \qquad (B-14)$$

According to (5) and (6), we need

$$\left.\begin{array}{l} P_x^{(0)}\left(b_\ell\right) = 1 - \exp\left(-v_\ell\right) e_{D-1}\left(v_\ell\right) \\[2mm] P_x^{(1)}\left(b_\ell\right) = 1 - Q_D\left(a, \sqrt{2v_\ell}\right) \end{array}\right\} \quad \text{for } 1 \leq \ell \leq L \quad , \qquad (B-15)$$

where normalized breakpoints

$$v_\ell \equiv \frac{b_\ell}{2\sigma_n^2} \quad \text{for } 1 \leq \ell \leq L \quad . \qquad (B-16)$$

Again $b_\ell \geq 0$ since x in (B-8) can never be negative.

Appendix C

PROGRAM FOR DETECTION AND FALSE ALARM PROBABILITIES

```
10   ! DETECTION CHARACTERISTICS FOR QUANTIZERS, GREATEST-OF, AND ACCUMULATOR
20   ! QUANTIZER OUTPUT (ORDINATE) LEVELS ARE SET AT 0,1,...,L;  L+1 LEVELS
30   ! QUANTIZER ABSCISSA BREAKPOINTS ARE ARBITRARY; L BREAKPOINTS
40      M=5           ! NUMBER OF TIME SAMPLES ACCUMULATED: M>=1
50      N=3           ! NUMBER OF INPUT CHANNELS SUBJECT TO OR-ING: N>=1
60      L=7           ! NUMBER OF NON-ZERO QUANTIZER OUTPUT LEVELS: L>=1
70   ! NORMALIZED ABSCISSA BREAKPOINTS OF QUANTIZER (L NUMBERS):
80      DATA 1.4,1.85,2.3,2.75,3.2,3.65,4.1
90      Dimax=4.5  ! MAXIMUM VALUE OF Di OF INTEREST
100     Distep=.5  ! INCREMENTS IN Di OF INTEREST
110     Np=6       ! SMALLEST PROBABILITY OF INTEREST IS 10^(-Np)
120     DIM X(1:1024),Y(1:1024),Axis(1:19)
130     DIM V(1:10),S(1:10),Pw(1:10),Pfa(1:1024)
140     REDIM V(1:L),S(1:L),Pw(1:L),Pfa(1:M*L)
150     READ V(*)
160     PRINTER IS 0
170     PRINT "NUMBER OF TIME SAMPLES ACCUMULATED:         M =";M
180     PRINT "NUMBER OF INPUT CHANNELS SUBJECT TO OR-ING: N =";N
190     PRINT "NUMBER OF NON-ZERO QUANTIZER OUTPUT LEVELS: L =";L
200     PRINT "    QUANTIZER OUTPUT (ORDINATE) LEVELS ARE SET AT 0,1,...,L."
210     PRINT "    QUANTIZER NORMALIZED (ABSCISSA) BREAKPOINTS ARE AT:"
220     FOR J=1 TO L
230     PRINT V(J);
240     NEXT J
250     PRINT
260     PRINT "INPUT VOLTAGE-SNR Di VARIES FROM 0 TO";Dimax;"IN STEPS OF";Distep
270     PRINT
280     PRINT "THE GRAPH BELOW GIVES THE (FALSE ALARM) PROBABILITY THAT THE"
290     PRINT "SYSTEM OUTPUT IS GREATER THAN OR EQUAL TO J, FOR J = 1 TO ML."
300     PRINT "THE INPUT SIGNAL-TO-NOISE RATIO IS ZERO FOR THIS GRAPH."
310     M0=M*L
320     M1=M0+1
330     M2=M/2
340     N1=N-1
350     FOR J=2 TO 10
360     Nf=2^J
370     IF Nf>M0 THEN 420
380     NEXT J
390     PRINT
400     PRINT "ARRAYS  X,Y,Pfa  ARE NOT DIMENSIONED LARGE ENOUGH"
410     STOP
420     REDIM X(1:Nf),Y(1:Nf)
430     FOR J=1 TO L
440     S(J)=FNPhi(V(J))^N1
450     NEXT J
460     FOR Di=0 TO Dimax STEP Distep
470     FOR J=1 TO L
480     Pw(J)=S(J)*FNPhi(V(J)-Di)        !       EQUATIONS 5 AND 21
490     NEXT J
500     MAT X=ZER
```

```
510    MAT Y=ZER
520    X(1)=Pw(1)          !        EQUATION 6;  Alpha(J) in X(J+1)
530    FOR J=2 TO L
540    X(J)=Pw(J)-Pw(J-1)
550    NEXT J
560    X(L+1)=1-Pw(L)
570    CALL Fft(Nf,X(*),Y(*))
580    FOR J=1 TO Nf              !        (X-iY)^M
590    T=(X(J)^2+Y(J)^2)^M2
600    A=M*FNArg(X(J),Y(J))
610    X(J)=T*COS(A)
620    Y(J)=-T*SIN(A)
630    NEXT J
640    CALL Fft(Nf,X(*),Y(*))
650    FOR J=1 TO M1
660    X(J)=X(J)/Nf               !        BETA OF FIGURE 7
670    NEXT J
680    IF Di>0 THEN 1220
690    PLOTTER IS "GRAPHICS"
700    GRAPHICS
710    Np1=Np+1
720    Np2=Np*2+1
730    Axis(Np1)=0
740    FOR J=1 TO Np
750    T=FNInvphi(.1^J)
760    Axis(Np1-J)=T
770    Axis(Np1+J)=-T
780    NEXT J
790    SCALE 0,M0,Axis(1),Axis(Np2)
800    FOR J=0 TO M0 STEP 5
810    MOVE J,Axis(Np2)
820    DRAW J,Axis(1)
830    NEXT J
840    FOR J=1 TO Np2
850    MOVE 0,Axis(J)
860    DRAW M0,Axis(J)
870    NEXT J
880    PENUP
890    T=0
900    FOR J=M1 TO 2 STEP -1
910    T=T+X(J)
920    I=J-1
930    IF (T>1E-11) AND (T<1-1E-11) THEN 960
940    Pfa(I)=100
950    GOTO 1050
960    A=FNInvphi(T)
970    Pfa(I)=A
980    PLOT I,A
990  ! GOTO 1050     !   TO ELIMINATE CROSSES, INSERT THIS INSTRUCTION
1000   MOVE I,A-Axis(Np2)*.008
```

```
1010    DRAW I,A+Axis(Np2)*.008
1020    MOVE I-.004*M0,A
1030    DRAW I+.004*M0,A
1040    PLOT I,A
1050    NEXT J
1060    PENUP
1070    DUMP GRAPHICS
1080    PRINT LIN(1)
1090    PRINT "THE GRAPH BELOW IS A PLOT OF DETECTION PROBABILITY VERSUS"
1100    PRINT "FALSE ALARM PROBABILITY, FOR THE VALUES OF Di GIVEN ABOVE."
1110    GCLEAR
1120    SCALE Axis(1),Axis(Np2),Axis(1),Axis(Np2)
1130    FOR J=1 TO Np2
1140    MOVE Axis(1),Axis(J)
1150    DRAW Axis(Np2),Axis(J)
1160    NEXT J
1170    FOR J=1 TO Np2
1180    MOVE Axis(J),Axis(Np2)
1190    DRAW Axis(J),Axis(1)
1200    NEXT J
1210    PENUP
1220    T=0
1230    FOR J=M1 TO 2 STEP -1
1240    T=T+X(J)
1250    IF (T<1E-11) OR (T>1-1E-11) THEN 1360
1260    B=Pfa(J-1)
1270    IF ABS(B)>7 THEN 1360
1280    A=FNInvphi(T)
1290    PLOT B,A
1300  ! GOTO 1360     !    TO ELIMINATE CROSSES, INSERT THIS INSTRUCTION
1310    MOVE B,A-Axis(Np2)*.008
1320    DRAW B,A+Axis(Np2)*.008
1330    MOVE B-Axis(Np2)+.008,A
1340    DRAW B+Axis(Np2)+.008,A
1350    PLOT B,A
1360    NEXT J
1370    PENUP
1380    NEXT Di
1390    DUMP GRAPHICS
1400    PRINT LIN(6)
1410    PRINTER IS 16
1420    END
1430    !
1440    DEF FNArg(X,Y)              ! PRINCIPAL ARGUMENT  OF X+iY
1450    IF X=0 THEN A=.5*PI*SGN(Y)
1460    IF X<>0 THEN A=ATN(Y/X)
1470    IF X<0 THEN A=A+PI*(1-2*(Y<0))
1480    RETURN A
1490    FNEND
1500    !
```

```
1510    DEF FNPhi(X)                    ! CUMULATIVE GAUSSIAN DISTRIBUTION
1520    IF ABS(X)>5.14 THEN 1780
1530    A=.282842712475*X
1540    C=COS(A)
1550    S=SIN(A)
1560    B=2*C
1570    A=B*C-1
1580    C=A*(1.2536751E-18+B*7.10005E-20+A*7.4517E-21)
1590    C=A*(1.533423425E-16+B*1.01649277E-17+C)
1600    C=A*(1.36760444757E-14+B*1.0601364636E-15+C)
1610    C=A*(8.89786526722E-13+B*8.06068838945E-14+C)
1620    C=A*(4.22616144318E-11+B*4.46968229249E-12+C)
1630    C=A*(1.46660614234E-9+B*1.80848587810E-10+C)
1640    C=A*(3.72252349369E-8+B*5.34275027603E-9+C)
1650    C=A*(6.91927520325E-7+B*1.15330990944E-7+C)
1660    C=A*(9.43281169838E-6+B*1.82066316364E-6+C)
1670    C=A*(9.44909268810E-5+B*2.10404583073E-5+C)
1680    C=A*(6.97183792408E-4+B*1.78228016255E-4+C)
1690    C=A*(3.80150767985E-3+B*1.10860645342E-3+C)
1700    C=A*(.0153985726157+B*.00507906961220+C)
1710    C=A*(.0467755234325+B*.0172439625887+C)
1720    C=A*(.108630245023+B*.0439773381941+C)
1730    C=A*(.201339747265+B*.0869894549959+C)
1740    C=A*(.330501521917+B*.144227226362+C)
1750    C=.703225002744+B*.247255168140+C
1760    Phi=.5+.0450158158079*X+.5*S*C
1770    GOTO 1920
1780    IF X>7 THEN 1910
1790    N=MAX(6,INT(69/ABS(X)),INT(525/X^2))+1
1800    A=1
1810    S=1
1820    B=1/X
1830    C=B*B
1840    FOR J=1 TO N
1850    A=(1-2*J)*A*C
1860    S=S+A
1870    NEXT J
1880    Phi=.398942280401*EXP(-.5*X*X)*ABS(B)*S
1890    IF X>0 THEN Phi=1-Phi
1900    GOTO 1920
1910    Phi=1
1920    RETURN Phi
1930    FNEND
1940    !
```

```
1950    DEF FNInuphi(Z)            ! INVERSE CUMULATIVE GAUSSIAN DISTRIBUTION
1960    X=2*Z-1
1970    DIM T(0:20),A(0:20)
1980    DATA .992885376619,.120467516143,.0160781993421,.00268670443716
1990    DATA .49963473024E-3,.988982186E-4,.2039181276E-4,.432727162E-5
2000    DATA .93808141E-6,.20673472E-6,.461597E-7,.1041668E-7,.23715E-8
2010    DATA .54393E-9,.12555E-9,.2914E-10,.679E-11,.159E-11,.37E-12
2020    DATA .912158803418,-.0162662818677,.43355647295E-3,.21443857007E-3
2030    DATA .262575108E-5,-.302109105E-5,-.1240606E-7,.6240661E-7,-.54012E-9
2040    DATA -.142321E-8,.3438E-10,.3358E-10,-.146E-11,-.81E-12,.5E-13,.2E-13
2050    DATA .956679709020,-.0231070043091,-.00437423609751,-.57650342265E-3
2060    DATA -.1096102231E-4,.2510854702E-4,.1056233607E-4,.275441233E-5
2070    DATA .43248450E-6,-.2053034E-7,-.4389154E-7,-.1768401E-7,-.399129E-8
2080    DATA -.18693E-9,.27292E-9,.13282E-9,.3183E-10,.167E-11,-.204E-11
2090    DATA -.965E-12,-.22E-12
2100    B=ABS(X)
2110    IF ABS(X)>=.8 THEN B=SQR(-LOG((1-X)*(1+X)))
2120    IF ABS(X)<.8 THEN 2220
2130    IF ABS(X)<.9975 THEN 2180
2140    Nmax=20
2150    RESTORE 2050
2160    Y=-.559457631330*B+2.28791571626
2170    GOTO 2250
2180    Nmax=15
2190    RESTORE 2020
2200    Y=-1.54881304237*B+2.56549012315
2210    GOTO 2250
2220    Nmax=18
2230    RESTORE 1980
2240    Y=X*X*3.125-1
2250    REDIM A(0:Nmax)
2260    READ A(*)
2270    Y2=Y*2
2280    T(0)=1
2290    T(1)=Y
2300    FOR N=2 TO Nmax
2310    T(N)=Y2*T(N-1)-T(N-2)
2320    NEXT N
2330    R=0
2340    FOR N=Nmax TO 0 STEP -1
2350    R=R+A(N)*T(N)
2360    NEXT N
2370    Inuphi=SGN(X)*B*R*1.41421356237
2380    RETURN Inuphi
2390    FNEND
2400    !
2410    SUB Fft(N,X(*),Y(*))    !    FFT SUBROUTINE HERE
```

Appendix D

ANALYSIS FOR GENERAL QUANTIZER

The characteristic function of decision variable z is still given by (8) in terms of f_y, the characteristic function of y. But now, from figures 5 and 2,

$$f_y(\xi) = \overline{\exp(i\xi y)} = \overline{\exp(i\xi q\{w\})} = \int_{-\infty}^{\infty} du\, p_w(u)\, \exp(i\xi q\{u\})$$

$$= \exp(i\xi h_0)\int_{-\infty}^{b_1} du\, p_w(u) + \ldots + \exp(i\xi h_L)\int_{b_L}^{\infty} du\, p_w(u)$$

$$= \exp(i\xi h_0)\, P_w(b_1) + \sum_{\ell=1}^{L-1} \exp(i\xi h_\ell)\left[P_w(b_{\ell+1}) - P_w(b_\ell)\right]$$

$$+ \exp(i\xi h_L)\left[1 - P_w(b_L)\right] \quad , \tag{D-1}$$

where P_w is the cumulative distribution function of random variable w, as given by (5). The inputs for this calculation of characteristic function f_z are M, N, L, $\{h_\ell\}_0^L$ and $\{b_\ell\}_1^L$. Again, input cumulative distribution functions $p_x^{(0)}$ and $p_x^{(1)}$ in (5) are arbitrary.

One problem with this quantizer is that P_D and P_F are stepwise functions of the decision threshold (which need not be integer now) at irregular points. A large DFT size would be necessary to track this behavior. However, operating characteristic plots of P_D vs. P_F would be smoother functions.

Appendix E

DERIVATION OF OPTIMUM PROCESSOR

We allow the signal, if present, to jump randomly and independently between input channels on each time sample. Let

$$Y(m) = \left\{ x_n(m) \right\}_{n=1}^{N} \quad \text{for } 1 \le m \le M \quad . \tag{E-1}$$

Under H_1, the probability density function of N-vector $Y(m)$ is

$$p^{(1)}(Y(m)) = \frac{1}{N} \left[p^{(1)}\left(x_1(m)\right) \, p^{(0)}\left(x_2(m)\right) \, \cdots \, p^{(0)}\left(x_N(m)\right) \right.$$

$$\left. + p^{(0)}\left(x_1(m)\right) \, p^{(1)}\left(x_2(m)\right) \, \cdots \, p^{(0)}\left(x_N(m)\right) + \cdots \right]$$

$$= \prod_{n=1}^{N} \left\{ p^{(0)}\left(x_n(m)\right) \right\} \frac{1}{N} \sum_{n=1}^{N} \frac{p_1\left(x_n(m)\right)}{p_0\left(x_n(m)\right)} \quad \text{for } 1 \le m \le M \quad . \tag{E-2}$$

Therefore the joint probability density function is

$$p^{(1)}(Y(1) \, \cdots \, Y(M)) = \prod_{m=1}^{M} \prod_{n=1}^{N} \left\{ p^{(0)}\left(x_n(m)\right) \right\} \prod_{m=1}^{M} \left\{ \frac{1}{N} \sum_{n=1}^{N} \frac{p^{(1)}\left(x_n(m)\right)}{p^{(0)}\left(x_n(m)\right)} \right\} \quad . \tag{E-3}$$

The likelihood ratio follows immediately as the last product in (E-3); the log-likelihood ratio is therefore

$$\ell n \text{ likelihood ratio} = \sum_{m=1}^{M} \ell n \left(\frac{1}{N} \sum_{n=1}^{N} \frac{p^{(1)}\left(x_n(m)\right)}{p^{(0)}\left(x_n(m)\right)} \right) \quad . \tag{E-4}$$

This result holds for arbitrary inputs with probability density functions $p(0)$ and $p(1)$.

When we employ the Gaussian example in (16), (E-4) simplifies to

$$\sum_{m=1}^{M} \ell n \left(\frac{1}{N} \sum_{n=1}^{N} \exp\left(\frac{d_i}{\sigma} x_n(m)\right) \right) \lessgtr \quad \text{threshold} \quad , \tag{E-5}$$

where data-independent scale factors have been absorbed in the threshold. Exact analysis of (E-5) is conceivable, but is exceedingly tedious. Also d_i and σ must be known in order to realize (E-5).

For $d_i > 2$, it may be shown, to a good approximation, that

$$\sum_{n=1}^{N} \exp\left(\frac{d_i}{\sigma} x_n(m)\right) \cong \exp\left(\frac{d_i}{\sigma} \max_n \{x_n(m)\}\right) \quad . \tag{E-6}$$

Substitution in (E-5) yields the approximate likelihood ratio test

$$\sum_{m=1}^{M} \max_n \{x_n(m)\} \gtrless \text{threshold} \quad . \tag{E-7}$$

Knowledge of d_i and σ is now not required. Processor (E-7) is just figure 1 or 5, with the quantizer replaced by a linear gain. This special case of (E-5) is very important, because decent performance can be obtained for $d_i > 2$, and this is exactly where (E-7) is virtually optimum. A good approximation to the performance of (E-7) is afforded by the results contained herein, if L is chosen large and the breakpoints are well-placed. Some approximate results via second-moment approaches are given in refs. 1, 10, 11, 12.

REFERENCES

1. A. H. Nuttall, "Signal-to-Noise Ratio Requirements for Greatest-Of Device Followed by Integrator," NUSC Technical Memorandum TC-13-75, 24 July 1975.

2. A. H. Nuttall, "Input Deflection Requirements for Quantizers Followed by Greatest-Of-Device and Integrator," NUSC Technical Memorandum TM No. 781174, 24 August 1978.

3. W. A. Struzinski, "OR-ing Loss Data for Square Law Detectors Followed by an OR-ing Device and an Accumulator," JASA, vol. 72, pp. 191-195, July 1982.

4. W. A. Struzinski, "OR-ing Loss for Quantizers Followed by an OR-ing Device and an Accumulator," IEEE Trans. on Acoustics, Speech, and Signal Processing, vol. ASSP-30, no. 4, pp. 668-671, August 1982.

5. W. A. Struzinski, "Optimizing the Performance of a Quantizer," submitted to JASA, October 1982.

6. A. H. Nuttall, "Numerical Evaluation of Cumulative Probability Distribution Functions Directly from Characteristic Functions," Proc. IEEE, vol. 57, no. 11, pp. 2071-2072, November 1969; also NUSL Report No. 1032, 11 August 1969.

7. A. H. Nuttall, "Alternate forms for Numerical Evaluation of Cumulative Probability Distributions Directly from Characteristic Functions," Proc. IEEE, vol. 58, no. 11, pp. 1872-1873, November 1970; also NUSC Report No. NL-3012, 12 August 1970.

8. Handbook of Mathematical Functions, U. S. Department of Commerce, National Bureau of Standards, Applied Mathematics Series 55, U. S. Government Printing Office, Washington DC, June 1964.

9. A. H. Nuttall, "Some Integrals Involving the Q_M-Function", NUSC Technical Report 4755, 15 May 1974.

10. "Loss of S/N Ratio in Peak Detecting N Channels of Data," ASW Technical Note, Hughes Aircraft Co., Fullerton, CA., 12 Feb. 1968.

11. J. J. Dow, B. M. Brown, N. A. Reeder, "A Performance Comparison of Three Narrowband Data Reduction Techniques," Tracor Report T70-AU-7382-C, Tracor Inc., Austin, TX, 16 July 1970.

12. D. F. Korff, "ORing," Raytheon Memo No. DFK:81/08, Raytheon Submarine Signal Division, Portsmouth, RI, 9 September 1980.

INITIAL DISTRIBUTION LIST

Addressee	No. of Copies
ASN (RE&S)	1
OUSDR&E (Research & Advanced Technology	2
Deputy USDR&E (Res & Adv Tech)	1
OASN, Dep Assist Secretary (Res & Adv Tech)	1
ONR, ONR-100, -102, -200, -400, -410, -422, -425, -425AC, -430,	9
CNO, OP-090, -098, -902, -941, -951, -951D, -951E,-952, -96, -981F, -981, -982F, -983	13
CNM, MAT-00, -05, SP-20, -24, ASW-12, -11, -13, -14, MAT-03621, Systems Project Office (PM-2) Trident, Surface Ships Project Office (PM-18)	11
DIA, DT-2C	1
NRL	1
NRL, USRD	1
NRL, AESD	1
NORDA	1
USOC, Code 241, 240	2
SUBBASE LANT	1
OCEANAV	1
NEOC	1
NWOC	1
NAVOCEANO, Code 02, 3400, 6200	3
NAVELECSYSCOM. ELEX 00. 03. 320	3
NAVSEASYSCOM, SEA-00, -05R, -611, -613, -62R, -63R-1, -631Y, -631Y (Surface Sys Sub-Gr), -92R, PMS 409-531 (W. Johnson)	10
NAVAIRDEVCEN	1
NAVAIRDEVCEN, Key West	1
NOSC	1
NOSC, Code 6565 (Library)	1
NAVWPNSCEN	1
NCSC	1
NAVCIVENGRLAB	1
NAVSWC	1
NAV SURFACE WEAPONS CENTER, WHITE OAK LAB	1
NAVTRAEQUIPCENT Technical Library	1
NAVPGSCOL	1
NAVAIRTESTCEN	1
APL/UW, SEATTLE	1
ARL/PENN STATE, STATE COLLEGE	1
CENTER FOR NAVAL ANALYSES (ACQUISITION UNIT)	1
DTIC	1
DARPA	1
NOAA/ERL	1
NATIONAL RESEARCH COUNCIL	1
WEAPON SYSTEM EVALUATION GROUP	1
WOODS HOLE OCEANOGRAPHIC INSTITUTION	1
ENGINEERING SOCIETIES LIB, UNITED ENGRG CTR	1
ARL, UNIV OF TEXAS	1
MARINE PHYSICAL LAB, SCRIPPS	1

TR 6815

Addressee	No. of Copies
INTERMETRICS INC. EAST LYME, CT	1
MAR, INC. EAST LYME, CT	1
EG&G WASHINGTON ANAL SER CTR, INC. (T. Russell)	1
HYDROTRONICS INC. (D. Clark)	1
ANALYSIS & TECHNOLOGY, INC., N. STONINGTON (T. Dziedzic)	1
EDO CORPORATION, NY (J. Vincenzo)	1
TRACOR CORP., AUSTIN, TX (J. Wilkinson)	1
Dr. David Middleton, 127 East 91st Street, New York, NY 10028	1
Prof. Louis Scharf, Dept. of Electrical Engin., University of Rhode Island, Kingston, RI 02881	1
Prof. Donald Tufts, Dept. of Electrical Engin., University of Rhode Island, Kingston, RI 02881	1
S. L. Marple, The Analytic Sciences Corp., 8301 Greensboro Drive, McLean, VA 22102	1
T. E. Barnard, Chesapeake Instrument Div., Gould Inc., Glen Burnie, Md 21061	1
Prof. P. M. Schultheiss, Dept. of Electrical Engin., P.O. Box 2157, Yale University, 15 Prospect Street, New Haven, CT 06520	1
Dr. Allan G. Piersol, Bolt, Beranek, and Newman, 21120 Van Owen St., P.O. Box 633, Canoga Park, CA 92305	1
Prof. Y. T. Chan, Dept. of Electrical Engin., Royal Military College, Kingston, Ontario, Canada K7L 2W3	1
Jim Hughen, EGG, 8809 Sudley Rd., Manassas, VA, 22110	1